https://doi.org/10.5194/egusphere-2026-4958
Preprint. Discussion started: 3 September 2026

Pressure-, temperature- and water-dependent melting in silica-rich rocks – new parameterization and its application in models of porous melt flow

Petra Maierová[1], Pavla Štípská[1], Pavlína Hasalová[1], Karel Schulmann[1], Roberto Weinberg[2], and Ondřej Souček[3]

[1]Czech Geological Survey, Klárov 3/131, 118 00, Prague 1, Czech Republic.
[2]School of Earth Atmosphere and Environment, Monash University, Clayton, Victoria 3800, Australia
[3]Mathematical Institute, Faculty of Mathematics and Physics, Charles University, Sokolovská 83, Prague 8, Czech Republic.

Correspondence: Petra Maierová (petra.maierova@geology.cz)

Abstract. Melting of the continental crust and transport of melt through it are key processes in the continental crust. Progress in numerical modeling of these processes is hindered by challenges in implementing the complex melting reactions that occur in crustal rocks. Here, we propose a description of the melting of micaceous silica-rich rocks based on a simplified parameterization of existing thermodynamic models and experimental data. In this parameterization, the equilibrium melt fraction depends only on the temperature, pressure, and bulk rock water content. It can be implemented in numerical models, is computationally efficient, and can be tuned to approximate the melting of different metasedimentary and metaigneous rock types. Besides melt productivity, it determines the water content in the solid matrix and melt, which can be used to estimate melt viscosity. We demonstrate the applicability of such parameterization on one-dimensional models representing porous melt flow through vertical crustal columns at various conditions. We show that long-lasting porous melt flow typically results in stratification with a low melt fraction in deep levels and melt accumulation at shallow levels of the partially molten column. In the melt source region, the water content decreases and heterogeneities disappear. In contrast, in shallow levels of the partially molten column, melt inflow from below causes heterogeneous enrichment in water content. In addition, due to the decrease of melt viscosity with pressure, the porous melt flow efficiency increases with depth. At deep-crustal conditions, the melt flow may be efficient already at ∼5–10% melt fraction.

1 Introduction

Melting and melt transport are key processes modifying the structure and composition of the continental crust (e.g., Brown et al., 2011; Sawyer et al., 2011). Several melt transport mechanisms have been described based on geological evidence, such as dyking (e.g., Petford et al., 1994; Weinberg and Regenauer-Lieb, 2010), melt segregation and flow through leucosomes in migmatites (e.g., Weinberg, 1999; Sawyer, 2001) and pervasive melt flow through microscopic pores along grain boundaries (e.g., Hasalová et al., 2008b; Štípská et al., 2019; Stuart et al., 2016; Chatterjee et al., 2024). Despite the wealth of geological data and numerous conceptual models, a comprehensive picture of melt transport in the crust is still lacking.

https://doi.org/10.5194/egusphere-2026-4958
Preprint. Discussion started: 3 September 2026

Numerical modeling is a valuable tool in this respect, as it can help to assess the style and efficiency of the melt transport mechanisms in different settings and their potential role in crustal differentiation. However, models often focus on particular aspects of melting and melt transport. For example, melt transport itself has been modeled without taking into account the melt generation and solidification (e.g., studies of porous melt flow in visco-plastic material (Keller et al., 2013); continuum approximation of dyking (Li et al., 2023); flow in porosity waves to explain pegmatite formation (Plunder et al., 2022)). Another group of models accounts for melting but not for the related chemical changes. These models typically define the melt fraction depending on temperature, pressure and protolith composition, usually based on laboratory experiments (e.g., models of magmatic intrusions (Gorczyk and Vogt, 2018; Cao et al., 2016); formation of partially molten zones in the deep crust (Annen et al., 2006); melt-induced diapirism and convection (Babeyko et al., 2002; Louis-Napoléon et al., 2024)).

In contrast, the impact of melt transport on crustal composition can be properly addressed only in models that include chemical aspects of melting and solidification. The melting reaction in multicomponent material inevitably induces changes in chemical compositions of the remaining solid and resulting melt (e.g., Hasalová et al., 2008b; Pavan et al., 2021). The subsequent melt motion through the solid modifies the local bulk composition of the partially molten rock, affecting its melting properties — a process referred to as the reactive melt flow (e.g., Jackson et al., 2018). Models of this process therefore require a definition of equilibrium melt fraction for a continuously changing chemical composition. While for a fixed composition, it is possible to calculate the melt fraction based on petrological (thermodynamic) simulations, such an approach would be computationally extremely demanding in a system with reactive melt flow. Besides the computation of the melt fraction, this "brute-force" approach would require tracking of multiple chemical components that define the composition of the rock. Despite significant progress in computational capabilities and recent efforts in this direction (Kerswell et al., 2024; Riel et al., 2022; Rummel et al., 2020), self-consistent thermo-mechanical-petrological models of melt transport through the crust are lacking. Moreover, in such a complex system, it may be difficult to understand the relationships between the individual model parameters and to interpret the resulting behavior. It is therefore useful to adopt an alternative approach – a parameterized description of melting based on knowledge of its key characteristics.

Various parameterizations of crustal melting have been adopted in numerical models of the reactive melt flow. In the simplest approximation, the melt fraction can be computed by the lever rule from the solidus and liquidus curves that (near-)linearly depend on the composition represented by a single variable (Schmeling et al., 2019, 2023; Maierová et al., 2023). This approach can be interpreted as an approximation of a solid solution of two endmember components that differ in their melting temperatures, where the "composition" variable is the proportion of one of them. More complicated quadratic formulas for the solidus and liquidus curves were proposed as an approximation of solid-solution and eutectic melting (Solano et al., 2014). In later studies, the approximate eutectic phase diagram was interpreted in terms of the SiO_2 content and compared with the real rock record (Jackson et al., 2018; Hu et al., 2022; Booth et al., 2024).

Alongside the research of crustal melting and melt transport, analogous processes in the mantle have been modeled (review by Katz et al., 2022) and various parameterizations of mantle melting have been applied (e.g., Katz and Weatherley, 2012; Keller and Katz, 2016). A notable case is the widely used thermodynamics- and experiment-based parameterization by Katz et al. (2003) that includes not only the effects of pressure and temperature but also of the water content.

https://doi.org/10.5194/egusphere-2026-4958
Preprint. Discussion started: 3 September 2026

The role of water in the reactive melt transport in crustal rocks has not yet been studied numerically; all the advanced melting parameterizations focused solely on the role of SiO_2 (Jackson et al., 2018; Hu et al., 2022; Booth et al., 2024). This implies a gap in our understanding of crustal melting systems, as many geological, theoretical and experimental studies have demonstrated that water (H_2O) is the key factor that controls the melt productivity of crustal rock types (for summary see Weinberg and Hasalová, 2015). Similarly to the case of SiO_2, the H_2O component partitions unevenly between the solid and melt, and the equilibrium melt fraction therefore changes with the amount of H_2O, which is a prerequisite for reactive melt flow. Water-dominated melting can occur already at temperatures around 650 °C (e.g., Vielzeuf and Schmidt, 2001; Weinberg and Hasalová, 2015)), which is significantly lower than the minimum solidus temperature of 850 °C assumed in the models of SiO_2-dominated melting (Jackson et al., 2018; Hu et al., 2022; Booth et al., 2024).

Water can be present as a free fluid phase or as an H_2O component bound in hydrous minerals or in the melt. In a closed system, the availability of water for melt production mainly depends on dehydration reactions that release H_2O from minerals, because rocks typically contain only a small amount of pore fluid water (e.g., Thompson, 1982; White and Powell, 2002). Above the wet solidus, it is expected that water can be added as a free fluid phase only at near-solidus conditions, because all H_2O will be immediately consumed by melt-producing reactions (e.g., White and Powell, 2002). The addition of H_2O in a rock above the wet solidus can occur by the addition of hydrous melt (White and Powell, 2002; Štípská et al., 2019).

Vielzeuf and Schmidt (2001) suggested that melting in silica-rich rocks may be approximately described in a binary system including an anhydrous rock component and H_2O component, and involving reactions between two anhydrous mineral phases, two hydrous mineral phases (e.g., muscovite and biotite), aqueous fluid phase, and melt. We build on this idea to define a new parameterization of the melt productivity of silica-rich rocks, depending on pressure, temperature and water content (free fluid phase and H_2O bound in hydrous minerals). We compare the melt fractions predicted using this parameterization with the results of petrological phase-equilibria models (Section 2). We focus on micaceous silica-rich rocks, as an abundant rock type in the continental crust, which produces granitic melts. Extending our approach to silica-poor rocks could be a focus for future work.

We demonstrate the parameterization's applicability in models of reactive porous melt flow through a vertical rock column (Section 3). We study the character of melt flow for different rock types (metapelite, metagranite), water contents and for different positions within the crust, i.e., different pressures (Section 4). Finally, we discuss the results in the frame of observed characteristics of formerly partially molten rocks in the continental crust (Section 5).

2 Melting parameterization

We introduce a simple parameterization of the melting of silica-rich rocks that can be used in thermo-mechanical numerical simulations. Silica-rich rocks, containing $SiO_2 > 63\,\mathrm{wt\%}$, are typically quartzo-feldspathic with a variable proportion of micas (muscovite, biotite) and may be of igneous, sedimentary or metamorphic origin. Following previous experimental and thermodynamic-modelling studies (e.g., Clemens and Vielzeuf, 1987; Vielzeuf and Schmidt, 2001; Johannes and Holtz, 1996; White and Powell, 2002; White et al., 2001; Holland and Powell, 2001; Gardien et al., 1995), we assume that the whole-rock

https://doi.org/10.5194/egusphere-2026-4958
Preprint. Discussion started: 3 September 2026

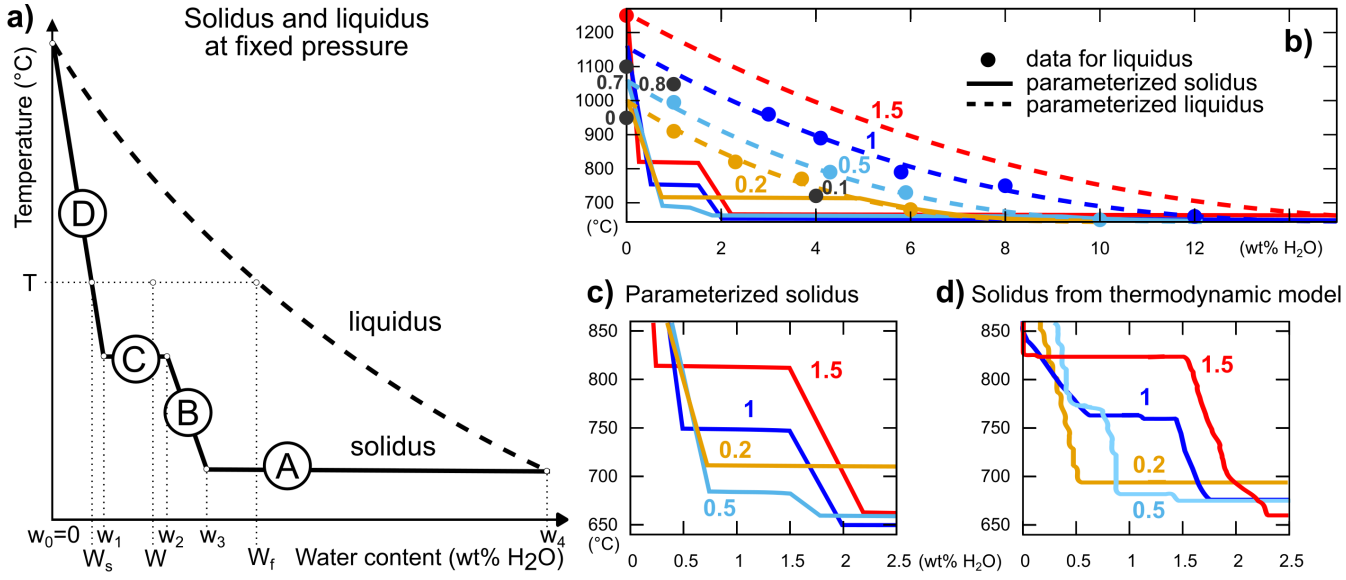

Figure 1. Melting parameterization. a) Scheme of melting parameterization at a fixed pressure. Solidus is described by a curve composed of four linear segments (A, B, C, D). Liquidus is an analytical function approximating experimental data. b) Example of the parameterized solidus and liquidus for different pressures (coded by colors and numbers, in GPa). For the solidus curve we use the following values of parameters that define the solidus as described in the text: $w_{01} = 0.5$, $w_{02} = 1.5$, $w_{03} = 2.0$, $w_{P1} = -0.5$, $w_{P2} = 0.0$, $w_{P3} = 0.4$; all in wt% H_2O. w_4 is the intersection point between the solidus and the liquidus at high W. Dots show experimental data for liquidus that were used for the fit of the analytical function (Makhluf et al. (2017), their Fig. 7; estimated dry solidus from Holtz et al. (2001), their Fig. 3; estimated eutectic points from Holtz et al. (2001), their Fig. 4). The liquidus function is $W_{f,\mathrm{wt\%\,H_2O}} = (aP_{\mathrm{GPa}}+b)\left(1-[(T_{^\circ\mathrm{C}}-c)/(d+eP_{\mathrm{GPa}})]^f\right)$, with fitted parameters: $a = 7.5\,\mathrm{wt\%\ H_2O\,GPa^{-1}}$; $b = 8.4\,\mathrm{wt\%\ H_2O}$; $c = 644\,^\circ\mathrm{C}$; $d = 316\,^\circ\mathrm{C}$; $e = 198\,^\circ\mathrm{C\,GPa^{-1}}$; $f = 0.41$. c) Closer view of the parameterized solidus. d) Solidus lines from thermodynamic computations using MAGEMin software (Riel et al., 2022) for the bulk-rock composition of "world-median pelite" (Forshaw and Pattison, 2023).

water content is the key factor that determines the melt productivity of these rocks, but we are aware that other factors, such as exact rock chemical compositions, also affect the melt productivity (White et al., 2011). As a first approximation, we neglect these effects and focus solely on the role of the H_2O component (the water content).

In rocks, H_2O can be present in hydrous minerals and as free fluid. In the melt, H_2O is dissolved. In our melting parameterization, we introduce the parameter W that represents the total wt% of H_2O in the partially molten rock (both in solid and melt). We assume that during partial melting, continuous reactions involving biotite and (to a minor extent) muscovite occur. In addition, a reaction corresponding to the terminal breakdown of muscovite occurs (hereafter called "muscovite breakdown"), which can cause a significant and abrupt increase in melt fraction.

The building blocks of the parameterization are the solidus and liquidus temperatures that depend on pressure P and water content W (Fig. 1). The shapes of the parameterized solidus and liquidus are defined to capture the main features of the results of thermodynamic computational models and experiments, as described below.

https://doi.org/10.5194/egusphere-2026-4958
Preprint. Discussion started: 3 September 2026

For a fixed pressure, the solidus temperature is approximated by a combination of four linear segments (Fig. 1a): segment A: wet solidus; segment B: continuous reaction where usually small amounts of muscovite and biotite gradually react to form melt along a wide temperature interval; segment C: muscovite breakdown, where all remaining muscovite rapidly reacts along a narrow temperature interval and is consumed; and segment D: continuous reaction where other hydrous minerals (e.g., biotite) gradually react to form melt (c.f. Vielzeuf and Schmidt, 2001).

The wet solidus defines the occurrence of the first droplets of melt under water-saturated conditions. We approximate it by a pressure-dependent function (see line A in Fig. 2; Holland et al., 2018; Holtz et al., 2001):

$$\begin{aligned} T_{\mathrm{ws},^\circ\mathrm{C}} &= 650 + 150\,(P_{\mathrm{GPa}} - 1)^4 \quad \text{for} \quad P < 1\,\mathrm{GPa}, \\ T_{\mathrm{ws},^\circ\mathrm{C}} &= 650 + 50\,(P_{\mathrm{GPa}} - 1)^2 \quad \text{for} \quad P \geq 1\,\mathrm{GPa}, \end{aligned} \tag{1}$$

The conditions of the muscovite terminal breakdown reaction are approximated according to thermodynamic models (see line C Fig. 2; Holland et al., 2018):

$$T_{\mathrm{mu},^\circ\mathrm{C}} = 620 + 130 P_{\mathrm{GPa}}\,. \tag{2}$$

The wet solidus and muscovite terminal breakdown temperatures are theoretically independent of water content, and they appear constant in Fig. 1a.

The endpoints of the linear segments of the solidus curve are defined by the values of w_1, w_2 and w_3 (Fig. 1a) that have to be tuned according to the modeled rock type, for example by comparison with thermodynamic computations (Fig. 1c,d). They are related to the ability of the rock to grow hydrous minerals, which in turn depends on the chemical composition of the rock. The value of w_3 represents the total amount of H_2O that may be stored in hydrous minerals in the rock. Typical values in silica-rich (meta)igneous rocks are $0.5 - 1$ wt% (e.g., Bonin et al., 2020). In (meta)pelitic rocks, this value can be up to $\sim$3 wt% (e.g., Forshaw and Pattison, 2023). When W is higher than w_3, in unmolten rock it corresponds to the situation where free water is present. The length of the w_1 to w_2 segment defines the potential increase of the melt fraction due to the muscovite terminal breakdown. The value of w_1 approximates the amount of water stored in minerals other than muscovite. We assume that these minerals undergo continuous melt-producing reactions. The values of w_1, w_2 and w_3 in the model may depend on pressure. For simplicity, we define them as linear functions of pressure:

$$w_{1,2,3} = w_{0;1,2,3} + w_{P;1,2,3}(P/P_0 - 1) \tag{3}$$

where $P_0 = 1$ GPa is the reference pressure. Parameter w_{P3} is positive and mimics the increasing water content bond in minerals with increasing pressure (Fig. 1c,d). The values of w_{P1} and w_{P2} determine the melt fractions in the vicinity of the muscovite breakdown. For some applications, the pressure dependences of $w_{1,2,3}$ may be neglected, as this simplification still predicts reasonable melt productivity, see Supplementary Fig. S1.

The liquidus temperature is approximated based on experiments of haplogranite melting (Holtz et al., 2001; Makhluf et al., 2017) (dots in Fig. 1b). These experiments show that the liquidus temperature decreases with increasing water content and increases with pressure. To capture these variations, we fitted the experimental data with an analytical relationship. The quality of the fit is visually assessed in Fig. 1b (see dots for experimental data and dashed lines for the analytical relationship).

https://doi.org/10.5194/egusphere-2026-4958
Preprint. Discussion started: 3 September 2026

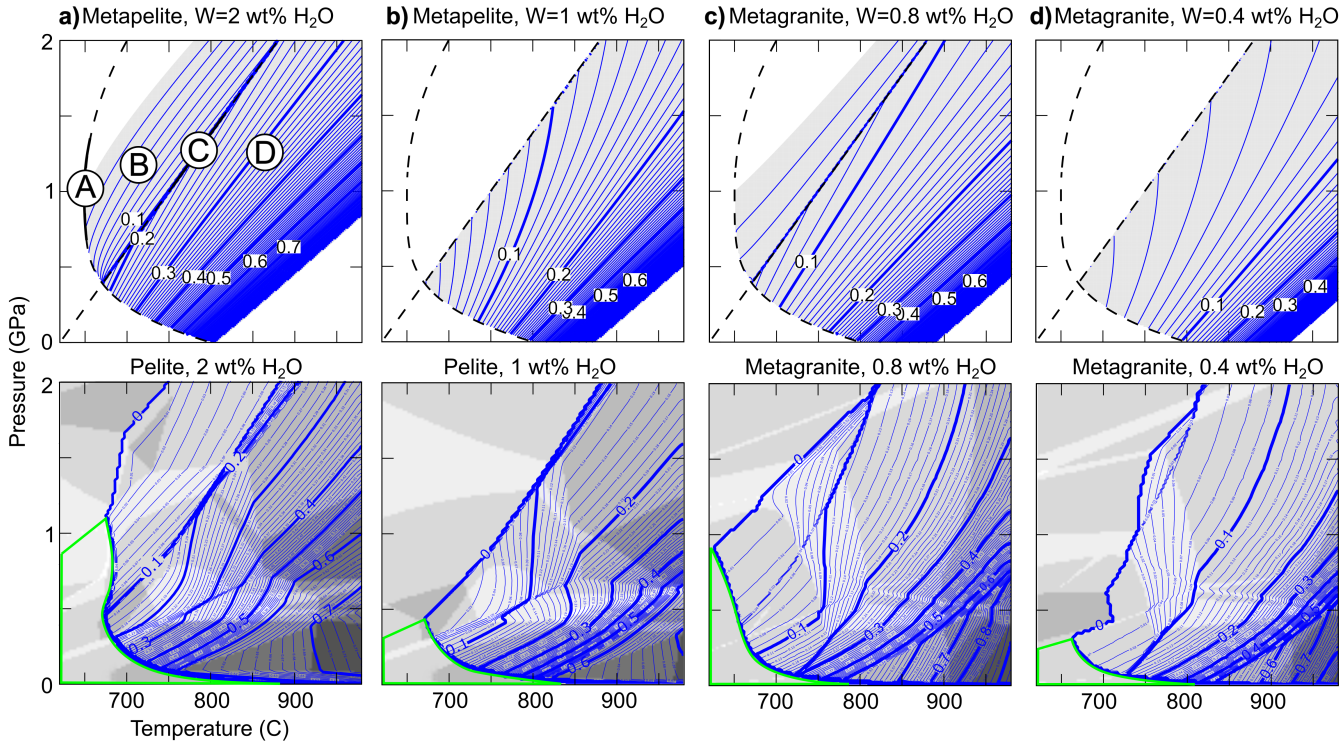

Figure 2. Melt fractions from parameterization and thermodynamic models for different rock types and water contents. Upper row of panels: results calculated from the parameterization with different $w_{1,2,3}$ and W. Parameters for "metapelite": $w_{01} = 0.5$, $w_{02} = 1.5$, $w_{03} = 2.0$, $w_{P1} = -0.5$, $w_{P2} = 0.0$, $w_{P3} = 0.4$; for "metagranite": $w_{01} = 0.2$, $w_{02} = 0.6$, $w_{03} = 0.8$, $w_{P1} = -0.2$, $w_{P2} = 0.0$, $w_{P3} = 0.4$; all in wt% H_2O. Blue contours show melt fraction. Black dashed lines show parameterized wet solidus (A) and muscovite breakdown reaction (C). B and D are regions where gradual melting reactions take place. Lower row of panels: Phase-equilibria modeling results computed using MAGEMin software (Riel et al., 2022), with the thermodynamic dataset by White et al. (2014) for metapelite, and the updated dataset by Green et al. (2025), previously Holland et al. (2018), for metagranite. The blue contours show melt fractions. The green line is the limit of the region where free fluid water is present. The grey fields in the background show the stability of individual mineral assemblages, separated by boundaries where one mineral appears or disappears. Scripts that can be used to produce the upper panels and bulk rock compositions (world median pelite, Forshaw and Pattison (2023); metagranite, Hasalová et al. (2008b)) for thermodynamic computations are in the Supplementary Material.

In the partially molten rock, assuming chemical equilibrium between the solid and melt, the water content of the solid (W_s) lies on the solidus line and the water content of the melt (W_f) lies on the liquidus line. In our parameterization, the solidus and liquidus curves therefore define the water content of the solid (W_s) and melt (W_f) during partial melting at a given temperature and pressure (see Fig. 1a). Knowing the bulk water content W of the partially molten rock, we can use its definition,

$$W = W_s(1 - \phi_{\text{mass}}) + W_f \phi_{\text{mass}}\,, \tag{4}$$

https://doi.org/10.5194/egusphere-2026-4958
Preprint. Discussion started: 3 September 2026

to calculate the equilibrium melt (mass) fraction ϕ_{mass} by rearranging (4) into the so-called lever rule:

$$\phi_{\text{mass}} = \frac{W - W_s}{W_f - W_s}. \tag{5}$$

Results of such calculations for selected rock types (defined by w_1, w_2, w_3) and bulk water contents (values of W) are shown in Fig. 2, upper row of panels. The values of $w_{1,2,3}$ that define the solidus curve are tuned according to thermodynamic computational models (Fig. 2, lower row of panels). The comparison of the panels in the upper and lower rows shows how our simple parametrization reproduces key characteristics of the melting in complex thermodynamically modelled chemical systems. Here, we do not specifically compare our results to experiments, because it has already been demonstrated by the very first thermodynamic models of "granitic" melts (Holland and Powell, 2001; White et al., 2001) that they reproduce reasonably well all key results of experiments as listed below, including the dissolution of H_2O in melt (e.g., see summary by Johannes and Holtz (1996)). The thermodynamic models also reproduce major features of biotite and muscovite melting, with muscovite reacting over a much shorter temperature interval compared to biotite (e.g., Gardien et al., 1995). This implies that our results also approximate the melting of real rocks (for comparison of thermodynamic models, experiments and real rocks see discussion by White et al. (2011)).

Fig. 2 demonstrates that the parameterization reproduces the following key characteristics of the melting of felsic rocks:

- Melt fraction increases with temperature
- Melt fraction increases with water content (compare Fig. 2a and b, Fig. 2c and d)
- Melt fraction decreases with pressure
- At medium- and high-pressure conditions, the solidus temperature depends on the water content in the rock: with progressively lower water content than that necessary for melting at the wet solidus, the solidus moves progressively to higher temperature (the so-called H_2O-undersaturated solidus).
- Prior to the muscovite breakdown, the melt fraction is low, only a few %, for a closed system (constant H_2O content) (field B in Fig. 2a)
- When crossing the muscovite breakdown, there is an abrupt increase in melt productivity that depends of the modal volume of muscovite (line C in Fig. 2a)
- The melt productivity of "metapelitic" rock types with a higher proportion of micas is higher than that of the "metagranitic" rock type at similar conditions (pressure, temperature and water saturation; compare Fig. 2a and c, Fig. 2b and d)

2.1 Limitations and validity range

The simple parameterization does not capture all characteristics of melt generation in silica-rich crustal rocks, because the equilibrium melt fraction depends on many factors other than just pressure, temperature and water content (White et al., 2011).

https://doi.org/10.5194/egusphere-2026-4958
Preprint. Discussion started: 3 September 2026

Namely, it is the whole rock composition that determines the mineral assemblage that is stable at variable pressure–temperature (P—T) conditions. It therefore controls the specific mineral reactions that occur along a particular P–T path, especially those involving water, and therefore melt productivity.

In the parameterization, multiple melt-producing reactions are not taken into account. Despite this omission, the model closely matches thermodynamic modeling results across most geologically common crustal P–T conditions. A significant discrepancy occurs at very low pressures and high temperatures (bottom-right corner of the panels in Fig. 2), where the parameterization predicts a higher melt fraction than the thermodynamic computations. Besides that, at high pressures (more than $\sim$2 GPa), the reliability of the parametrized melt fractions is limited due to the deteriorating precision of the underlying thermodynamic models (Holland et al., 2018). In summary, the parameterization can be applied across the range of P–T conditions relevant to crustal melting, except the extremely low–P high–T conditions, which are uncommon in regional metamorphism and are more characteristic of localized contact metamorphism.

Note that in order to obtain a reasonable estimate of the melt productivity in a specific rock, it is crucial to choose a realistic value of the water content (W). Specifically, below the solidus, only a small fraction of free fluid phase can reside in the rock. Therefore, W should not exceed the amount of H_2O in hydrous minerals just before crossing the wet solidus, which varies substantially with pressure. The examples in Fig. 2a,c therefore show reasonable melt fractions for a rock that crossed the solidus at P$>\sim$1 GPa (i.e., above the domain bounded by the green contour that limits free fluid water presence). Likewise, in Fig. 2b,d, the calculated melt fractions are reasonable for a rock that crossed the solidus at P$>\sim$0.4 GPa.

The parameterization can be tuned for different whole-rock compositions and each pair of solidus and liquidus curves can then be used to calculate melt productivity. We demonstrate such an approach on two rock types – metapelite and metagranite – where we tuned values of $w_{1,2,3}$ defining the solidus curve. Metasedimentary rocks are dominant in subduction wedges of accretionary and collisional orogens. Metasedimentary rocks and metagranitoids are the main lithologies in the upper–middle part of the orogenic crust, which may be thickened to several tens of km. The proposed parametrization may be useful in models of melt generation and transport in these settings.

We note that reactive melt flow leads to changes in chemical composition (not just changes in the water content), which would correspond to the shift in $w_{1,2,3}$. The applicability of the parametrization in models with reactive melt flow is therefore limited by the chemical differences between the melt and the solid and by the amount of melt loss. Melt loss, melt transport and melt addition induce chemical changes particularly in the concentrations of the dominant melt-forming oxides. In metapelites, metagreywackes and granites, the melt loss results in a notable depletion of SiO_2, Na_2O and K_2O (e.g., Stepanov et al., 2025). For the melt loss of up to $\sim$20–30%, the resulting changes are relatively minor (Stepanov et al., 2025) allowing the contents of oxides critical for melt production to remain sufficiently high for continued melting. In other rock types, such as those with low SiO_2 contents, melt loss may decrease or inhibit further melt production; such rocks are not considered here.

https://doi.org/10.5194/egusphere-2026-4958
Preprint. Discussion started: 3 September 2026

3 Melt flow through a crustal column

To document the applicability of the presented parameterization, we implement it into a simple numerical model of porous melt flow. The model is one-dimensional (1D) and represents gravity-driven porous melt flow through a vertical column of rock in hot viscously-deforming silica-rich continental crust. The melt flow is reactive: the water content affects the melt productivity and, because the water content in the melt is higher than in the solid, and because the melt moves through the solid, there is a feedback between the melt motion and melt productivity. We investigate this feedback for a range of P–T conditions where the proposed parametrization is applicable, namely at pressures between 0.5 GPa and 2 GPa, and temperatures typically resulting to low to moderate melt fractions ($\lesssim$0.3).

3.1 Model design

The model is implemented using the open-source finite-element software ASPECT (Kronbichler et al., 2012; Heister et al., 2017; Dannberg and Heister, 2016; Dannberg et al., 2019; Bangerth et al., 2024a). Details of the numerical implementation of the porous melt flow were described by Dannberg and Heister (2016) and in the ASPECT manual (Bangerth et al., 2024b). Details of the solved equations, numerical implementation of melting and values of model parameters are given in the Appendix A; here we provide only a brief overview.

The porous melt flow is modelled using the two-phase flow formalism (McKenzie, 1984). It assumes that the material consists of a solid matrix that can support stress and an interconnected network of pores filled with melt. In real partially molten rocks, the solid matrix is made of mineral grains and the melt flows through microscopic pores along grain boundaries. The assumption of the solid matrix limits the applicability of this apprach, because above a certain melt-fraction threshold (∼25–50%), the granular matrix in rocks disintegrates and individual grains or clusters float in the melt, forming magma, thus having a different rheological behavior (e.g., Renner et al., 2000).

There are only two phases in the model – the solid and the melt – which implies that the melt entirely fills the pores in the matrix. Therefore, the volumetric melt fraction of the melt, ϕ, is the same as the porosity of the solid matrix. We note that for some conditions (typically at low P and high W; see Fig. 2), free fluid water may be present within the rock below the solidus. In our model, the mechanical or thermal effects of fluid water are not accounted for, and its motion through the solid is not simulated; it is assumed to be confined in the solid.

We assume thermal and chemical equilibrium between melt and solid at the spatial scale of the model resolution and time scale of the model time steps. That implies the same temperature in both of them and practically instantaneous (compared to the model time steps) adjustment of W_s and W_f to the values on the solidus and liquidus curves (Fig. 1a).

The two-phase flow formalism uses a macro-scale description of the porous flow where the properties of the pores – their sizes and shapes – are represented by the rock permeability, k_ϕ. The flow of the melt is then described by the Darcy law:

$$\mathbf{u}_{\mathrm{rel}} = \mathbf{u}_f - \mathbf{u}_s = \frac{k_\phi}{\eta_f \phi} \left(\rho_f \mathbf{g} - \nabla p_f \right) , \tag{6}$$

where u_{rel} is the relative velocity of the melt (u_f) with respect to the solid (u_s), η_f is the melt viscosity, ρ_f is the melt density, $\mathbf{g}$ is the gravity, p_f is the pressure in the melt and ∇ denotes the gradient. The Darcy law states that the porous melt flow (melt

https://doi.org/10.5194/egusphere-2026-4958
Preprint. Discussion started: 3 September 2026

percolation) through the solid is driven by pressure gradients in the melt and that its velocity increases with the permeability of the solid matrix and decreases with the viscosity of the melt. Alternatively, the Darcy law can be rewritten as:

$$\mathbf{u}_{\mathrm{rel}} = \frac{k_\phi}{\eta_f\,\phi}\left[(\rho_f - \rho_s)\mathbf{g} - \nabla p^*\right], \tag{7}$$

where the first term on the right-hand side expresses melt buoyancy due to the difference between the melt density (ρ_f) and solid density (ρ_s). The excess melt pressure $p^* = p_f - p_{\mathrm{lith}}$, where p_{lith} is the lithostatic pressure, is related to compaction and dilation of the porous rock matrix and to other non-lithostatic effects (Spiegelman et al., 2007).

In addition to the melt flow, we solve for deformation of the solid (the mass balance and conservation of momentum). In a 1D model, the deformation of the solid is highly restricted. Still, it plays a role because it is coupled with melt flow and melting due to mass conservation. The deformation of the solid in 1D therefore results from compaction and dilation of the solid due to melt percolation and due to volumetric changes associated with melting and solidification (right-hand side of Eq. (A3) in Appendix A).

The internal energy balance (heat equation) is solved, including the heat diffusion and advection and the latent heat of melting. We also track the water content in solid and melt as they are advected by their respective velocities and affected by melting and solidification. During the time evolution of the model, we have the variables ϕ, W_s and W_f from the previous time step as they are advected by the melt and solid. These "old" W_s and W_f are typically out of equilibrium, they do not lie on the solidus and liquidus, because P–T conditions change between model time steps and because the melt can move through the solid. The “old” values of ϕ, W_s and W_f define the bulk water content W of the partially molten rock (Eq. (4)). We therefore know the bulk water content W, and we adjust ϕ, W_s and W_f to their "ideal" values that lie on the solidus and liquidus curves, while keeping W fixed. This step represents melting or solidification. This procedure is described in detail in Appendix A3.

3.2 Model domain, initial and boundary conditions

The model domain is 10 km deep, vertically divided into 200 elements, quadratic in u_s, u_f, W_s, W_f and temperature and linear in pressure. The model is pseudo-1D: it is a one-element-wide stripe with thermally insulated impermeable free-slip side boundaries. Zero velocity is prescribed at the bottom boundary. The top boundary is open to balance volumetric changes due to melting/solidification. The vertical position of the column within the crust is mimicked by the pressure prescribed at the top boundary of the model, P_{top}.

The initial temperature is uniform in each model case. During the time evolution, the temperature at the top boundary, T_{top}, is fixed to the initial temperature. At the bottom boundary, a time-constant temperature, T_{bot}, is prescribed. It is higher than the initial temperature, which means that the early thermal state of the models is out of equilibrium – the temperature at the bottom boundary is significantly higher than just above the boundary. Due to the resulting high thermal gradient in the lowermost part of the domain and due to the relatively small spatial extent of model, the thermal equilibration is very fast and a nearly linear temperature profile develops in $\sim$1 Myr of evolution in all studied cases.

The initial melt fraction is zero, which implies, according to Eq. (4), $W(t=0) = W_s(t=0)$. In most models, the initial water content is prescribed to a constant value, W_0, except for the lowermost 1-km-thick layer where $W = 0$, representing a

https://doi.org/10.5194/egusphere-2026-4958
Preprint. Discussion started: 3 September 2026

dry rock. This dry layer is added artificially to ensure that no melt is generated at the bottom boundary. In selected models, we additionally prescribe an anomalous 2-km-thick middle layer with a different initial water content (increased or decreased to the value $W_{0,\mathrm{anom}}$). The transitions between the layers are smoothed using the logistic function. During the time evolution, the water content at the bottom boundary is fixed to zero. In all model cases, the temperature is below the solidus at the top and bottom boundaries.

3.3 Material properties

To fully determine the evolution of the model, we have to specify material properties, namely the parameters in the melting law, the densities of the solid and melt, the shear and bulk viscosities of the solid, the viscosity of the melt, the permeability and thermal parameters. We adopt a simple definition of most parameters and focus only on the properties affected by our melting parametrization, namely the melt productivity and melt viscosity, which depend on the water content (see below). The values of the material parameters are listed in Table A1 in Appendix A.

The details of the melting parameterization are described in Section 2. For numerical reasons, we prescribe a slight dependence of the wet solidus and muscovite breakdown on W: $T_{\mathrm{solidus}}(w_1) = T_{\mathrm{solidus}}(w_2)+5$ and $T_{\mathrm{solidus}}(w_3) = T_{\mathrm{solidus}}(w_4)+5$, in Kelvin.

The densities and thermal parameters are assumed to be constant and their values correspond to typical values for felsic crustal rocks. Namely, the density of the solid is $2800\,\mathrm{kg\,m^{-3}}$, the density of the melt is $2400\,\mathrm{kg\,m^{-3}}$ and the thermal conductivity is $3\,\mathrm{W\,m^{-1}K^{-1}}$. The density changes due to the presence of water and potential other chemical variations are neglected. Based on thermodynamic computations (Supplementary Material, Fig. S2), we expect that the density-dependent parameter that governs the rate of the melt percolation, $\rho_s - \rho_f$ in Eq. (6), may vary by a factor of 2 in real rocks.

To define the rheology of the partially molten rock, we use a simple temperature- and porosity-dependent flow law:

$$\eta_s = \eta_0 \exp\left(\frac{A}{RT}\right)\exp(-\alpha\phi) \tag{8}$$

where $\eta_0 = 10^{12}\,\mathrm{Pa\,s}$, $A = 150\,\mathrm{kJ\,mol^{-1}}$ and α =20 are parameters and R is the gas constant (Fig. S3 in Supplementary Material). The resulting viscosity varies between $10^{21}\,\mathrm{Pa\,s}$ and $10^{19}\,\mathrm{Pa\,s}$ in unmolten rock at $T = 600 - 900\,^{\circ}\mathrm{C}$, which is a value range commonly expected for deforming silica-rich middle-lower crustal rocks at these temperatures (e.g., Jamieson et al., 2011). Porosity has a major effect on the viscosity as the pores weaken the solid matrix. The exponential dependence on porosity in Eq. (8) is based on experimental data and theoretical considerations (see Keller et al., 2013; Katz et al., 2022, for a discussion). The value of $\alpha = 20$ is a modest estimate of this parameter and implies a viscosity drop by one order of magnitude due to a porosity increase of $\sim$10%. For high melt fractions, more complicated parametrizations were proposed (e.g., Costa et al., 2009) which, however, predict very low viscosities that would inevitably lead to numerical issues in the present models. Instead, we impose a lower constant cutoff value on viscosity ($10^{16}\,\mathrm{Pa\,s}$). The use of constant shear viscosity for high melt fractions is a common approach in numerical models of porous melt flow (e.g., Keller et al., 2013; Schmeling et al., 2019; Booth et al., 2024). We neglect other factors that may change rock rheology, such as brittle faulting or changes in viscosity due

https://doi.org/10.5194/egusphere-2026-4958
Preprint. Discussion started: 3 September 2026

to compositional variations. The use of simplified η_s is particularly valid for the 1D model, where solid motion is restricted to one direction and the influence of the solid viscosity on the model evolution is minor.

The bulk viscosity of the porous solid rock is defined relative to the shear viscosity:

$$\eta_b = \eta_s(\beta_1 + \beta_2/\phi) \tag{9}$$

The $1/\phi$ singularity of the η_b/η_s ratio for $\phi = 0$ is based on theoretical models (e.g., Simpson et al., 2010; Schmeling et al., 2012). The constants $\beta_1 = 2$ and $\beta_2 = 0.3$ (Maierová et al., 2023) are defined so that for a low porosity, the functional dependence is similar to the model by Schmeling et al. (2012), and for $\phi \to 1$, the ratio η_b/η_s is ~ 2 (Rudge, 2018). For high porosity, the minimum cutoff value of the shear viscosity implies a nearly constant bulk viscosity (Fig. S3 in Supplementary Material). Booth et al. (2024) demonstrated that this choice approximates well the impeding effect of small-scale convection on crystal settling in magma, thus capturing the basic characteristics of the solid and melt separation. The proposed modelling approach is therefore, to the first order, applicable to high-porosity "magmatic" regions.

The melt viscosity is, together with the rock permeability, the key property that determines the efficiency of melt flow through the rock (see the Darcy law, Eq. (6)). According to experiments, η_f decreases with temperature and water content (e.g., Schulze et al., 1996; Holtz et al., 2001; Whittington et al., 2004). In our model, the water content of the melt W_f is computed during the model run. We can therefore directly use an experimentally determined functional dependence for η_f (Schulze et al., 1996) (Fig. 3):

$$\eta_f = 10^{-2.5726+\left(23.4-13.2\,W_f^{0.11}\right)\frac{10^3}{RT}} \tag{10}$$

We note that the uncertainty in the melt viscosity is important as values computed according to experimentally derived relationships can span one order of magnitude (e.g., Schulze et al., 1996; Hess and Dingwell, 1996). Variations of the melt chemical composition (apart from water) induce viscosity variations of a similar order, if we consider felsic to intermediate melt types (Giordano et al., 2008). The silica content is the most important factor that increases the melt viscosity and may counteract the effect of water. According to the experimentally derived relationships, the effect of water is still dominant, and incorporation of the effect of silica would bring a second-order correction (e.g., Giordano et al., 2008, their Fig. 9).

The permeability depends on the porosity, spacing of the pores and their geometry. We use the definition of permeability proposed by Keller et al. (2013):

$$k_\phi = k_0 D^2 \phi^3 (1-\phi)^2\,, \tag{11}$$

where D is the spacing of the pores. If we assume that melt is distributed along grain boundaries, D corresponds to the grain size. The value of the permeability prefactor k_0 is relatively weakly constrained, ranging between 10^{-3} and 10^{-1}, where the lower values are based on theoretical studies and the higher values on experiments and observations (review by Katz et al., 2022). Here we prescribed the intermediate value, $k_0 = 10^{-2}$, and $D = 1\,\text{mm}$.

Among all the material parameters, it is the permeability that, in our view, is the source of the largest uncertainty in the model. It is the key parameter for porous melt flow and, at the same time, its description by Eq. (11) is a major simplification of the real

https://doi.org/10.5194/egusphere-2026-4958
Preprint. Discussion started: 3 September 2026

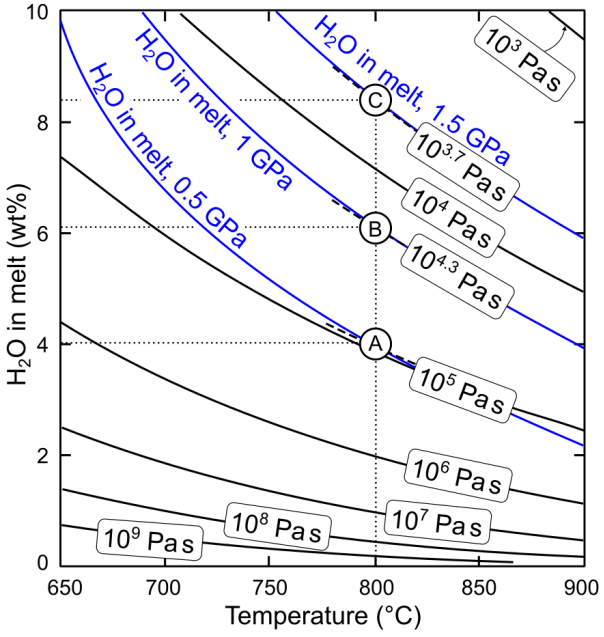

Figure 3. Viscosity of melt as an input parameter for the models. Black lines are contours of the melt viscosity (η_f) depending on the temperature and H_2O content (W_f) according to the experimentally derived relationship (10) by Schulze et al. (1996). Blue lines show the H_2O contents in melt at pressures 0.5, 1 and 1.5 GPa, as they depend on temperature, according to the liquidus function that relates W_f with T and P (see Fig. 1b). The blue lines show that more H_2O is dissolved in the melt at higher pressures, causing a lower viscosity at a given temperature. For example, at 800°C and 0.5 GPa (point A), there is 4 wt% H_2O in melt and $\eta_f \sim 10^5$ Pa s, while at the same temperature at 1 GPa (point B), there is ~6.1 wt% H_2O in melt and $\eta_f \sim 10^{4.3}$ Pa s, and at 1.5 GPa (point C), there is ~8.4 wt% H_2O in melt and $\eta_f \sim 10^{3.7}$ Pa s.

situation. In real rocks, permeability can vary in space and time, being determined by the width, connectivity and orientation of the pores. Due to rock heterogeneity, channeling of pores and variations in grain size, we expect that the permeability can vary by at least one order of magnitude for a given porosity.

4 Results

We perform a parametric study, where we focus on the effects of the realistic pressure- temperature- water-dependent melt productivity and variable melt viscosity. We vary the initial water content (W_0, $W_{0,\mathrm{anom}}$), rock type ("metapelite" and "metagranite", see Fig. 2), and pressure and temperature conditions (P_{top}, T_{top} and T_{bot}). For each presented model case, we show the results with melt percolation according to the two-phase flow equations, as well as the results where the melt is immobile in the solid ($k_\phi = 0$, $u_f = u_s$) and the water content W is, therefore, constant in time. For a selected reference case, we describe the time evolution of all important model variables and material properties (Fig. 4). In other cases (Figs 5–6), we focus on the melt distribution and water-content variations only (figures showing other variables and material properties are in the

https://doi.org/10.5194/egusphere-2026-4958
Preprint. Discussion started: 3 September 2026

Supplementary Material). To highlight the approximate character of the melting parameterization, in the text and figures that describe the numerical models, we omit the unit "wt% H_2O" of the variables W, W_s and W_f, and treat them as dimensionless quantities.

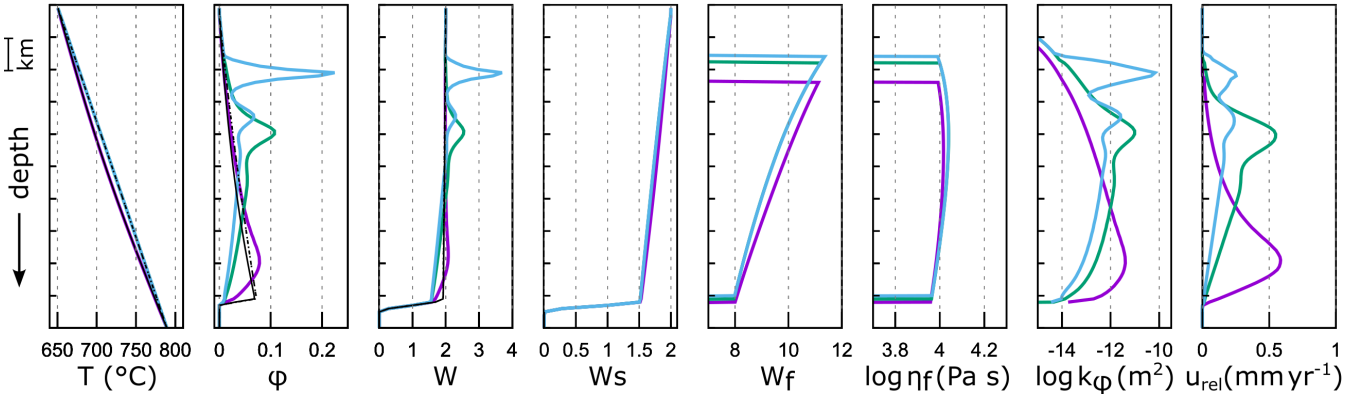

Figure 4. Reference model. Model parameters are: $P_{\rm top} = 1\,$GPa (resulting in pressure at the bottom boundary ~1.3 GPa), $T_{\rm top} = 650\,^{\circ}$C (that equals water-saturated solidus at 1 GPa), $T_{\rm bot} = 790\,^{\circ}$C. Parameters in the melting law are the same as in Fig. 2 for "metapelite"; $W_0 = 2$. Individual panels show variations of model properties (temperature T, melt fraction ϕ, bulk water content W, solid water content W_s, melt water content W_f, melt viscosity η_f, permeability k_ϕ and relative velocity between the melt and the solid $u_{\rm rel}$) with depth at three different time steps. Purple, green and blue lines show the results at 1, 5 and 10 Myr of model evolution. Solid, dashed and dotted black lines show the results for ϕ and W at 1, 5 and 10 Myr if melt percolation through the solid is switched off (for T, W_s, W_f and η_f, the result is visually the same as with melt percolation; k_ϕ and $u_{\rm rel}$ are zero by definition). Note that W is constant in this case.

4.1 Reference model case

First, we show a reference case with parameters $T_{\rm top} = 650\,^{\circ}$C, $T_{\rm bot} = 790\,^{\circ}$C, $P_{\rm top} = 1\,$GPa, $W_0 = 2$ and "metapelite" rock type (Fig. 4).

In the model, the temperature (T in Fig. 4) quickly departs from the initial 650 °C due to the hot bottom boundary condition ($T_{\rm bot} = 800\,^{\circ}$C). Already at $t = 1\,$Myr, a nearly linear temperature profile is established. Similar formation of a linear temperature profile over the first 1 to 2 Myr is observed in all modeled cases. In regions where T exceeds the solidus, melting occurs and melt percolates according to the Darcy law. During melting, local W_s and W_f follow the solidus and liquidus curves. As the melt moves, it transports water through the solid. As a result, the local bulk water content evolves over time (W in Fig. 4). Note that W_s and W_f do not change significantly during the simulation – it is the change in the proportion between the melt and the solid that causes changes in W (Eq. (4)).

Initially, the melt fraction (ϕ in Fig. 4) is the highest in the lowermost (warmest) part. With time, the melt flow towards shallow levels induces changes in local water content. W in shallow levels increases, inducing higher melt productivity there,

https://doi.org/10.5194/egusphere-2026-4958
Preprint. Discussion started: 3 September 2026

while the opposite process takes place in deep levels. The high melt fraction is localized in distinct peaks that travel upward through the domain, forming so-called porosity waves. The travel speed of the porosity waves is $\sim 1\,\mathrm{km\,Myr^{-1}}$ in this model.

Figure 4 further shows properties that affect the melt flow efficiency — W_f, η_f and k_ϕ — and the resulting velocity of melt through the solid, u_{rel}. The melt water content W_f follows the liquidus curve and therefore increases with pressure and decreases with temperature (Fig. 1a,b). The decrease of W_f with increasing depth (W_f in Fig. 4) demonstrates the dominance of temperature on the melt water content in the prescribed steep temperature gradient. The melt viscosity (η_f in Fig. 4) explicitly depends on the temperature and W_f (Eq. (10)). The temperature dependences of η_f and W_f effectively cancel out, leading to a nearly constant $\eta_f \approx 10^4\,\mathrm{Pa\,s}$.

The permeability (k_ϕ in Fig. 4) varies due to the varying porosity. For relatively low ϕ, it is approximately proportional to ϕ^3 (Eq. (11)). The melt flow is therefore more efficient in regions with a high melt fraction. The velocity of melt percolation (u_{rel} in Fig. 4) depends on the ratio between k_ϕ and η_f (Eq. (6)). In this model, it is typically around $0.5 - 1\,\mathrm{mm\,yr^{-1}}$, with the highest values correlating with regions with a high melt fraction.

Figure 4 also depicts results of a model where melt percolation through the solid is switched off, having otherwise the same parameters as the reference case (solid and dashed black lines in Fig. 4 for ϕ and W). Without melt percolation, W is constant in time, because both melt and solid are practically immobile in the 1D model. The resulting melt distribution then corresponds to the melt productivity for $W = W_0$ and varies with time only due to the conductively increasing temperature (black lines showing ϕ in Fig. 4). The melt fraction differs substantially from the case with melt percolation. With melt percolation, melt gathers in the shallow part of the partially molten domain, while without melt percolation the melt fraction shows a maximum near the bottom of the domain and decreases near-linearly upwards.

On the other hand, the melt percolation has only a minor effect on T, W_f and η_f. The effect on T is only through the heat advection and latent heat. The percolative melt motion is slow and both advection and the latent heat are proportional to the melt fraction, which is relatively low. Therefore, conduction, which is independent of melt flow, dominates the temperature evolution. As a result, material properties that depend mainly on T (i.e., η_f and W_f), are practically unaffected by the melt flow in this model; we omit them in Fig. 4 and show them only in the Supplementary Figures S4–S12.

4.2 Effect of melt productivity

We investigate in detail the effect of melt productivity as it depends on the rock type, initial water content and P–T conditions. We define five model cases (Fig. 5a-e): a) model where, due to slightly higher temperature compared to the reference case, muscovite breakdown occurs within the model domain; b) model with lower initial water content (W_0); c) model with "metagranite" rock type; and models similar to the reference model, but with an anomalous layer having an d) increased or e) decreased initial water content ($W_{0,\mathrm{anom}}$).

The parameters in the first model, Fig. 5a, are: $P_{\mathrm{top}} = 1\,\mathrm{GPa}$, $T_{\mathrm{top}} = 650\,^\circ\mathrm{C}$ and $T_{\mathrm{bot}} = 810\,^\circ\mathrm{C}$ and "metapelite" rock type, meaning that the only difference from the reference model is T_{bot} increased by 20°C. For these conditions, the muscovite breakdown takes place in the lower part of the model domain at $P \sim 1.2 - 1.3\,\mathrm{GPa}$. In models without melt percolation (black curves), the computed melt fraction directly corresponds to the melt productivity in Fig. 2a, showing a marked increase due

https://doi.org/10.5194/egusphere-2026-4958
Preprint. Discussion started: 3 September 2026

to the muscovite breakdown. If melt percolation is accounted for, the melt produced at depth moves upward, forming waves of increased melt fraction in shallower levels in a similar manner as in the reference case. The final distribution of W is, however, different from the reference model: the increased melt productivity due to muscovite breakdown in the lower part of the domain and the subsequent melt loss cause a decrease of W there. Eventually, a step in W develops at the depth of the muscovite breakdown.

The model in Fig. 5b has the same parameters as the one in Fig. 5a, except for the lower initial water content, $W_0 = 1$. In this case, while melt is produced in the lower part of the domain, the melt productivity is zero in the upper part, at conditions where muscovite is stable. The melt produced at depth cannot percolate efficiently into the unmolten material above and accumulates on top of the melt-productive region, causing local changes in W.

The model in Fig. 5c has the same P–T conditions as that in Fig. 5a,b but with "metagranite" rock type and $W_0 = 0.8$. In this case, the region with the increased melt productivity is overlain by a region with a relatively small, but non-zero melt fraction ($<5\%$). This is sufficient for melt percolation, formation of porosity waves and related variations in W similar as in the cases in Fig. 5a and Fig. 4. Due to somewhat lower melt productivity, the amplitudes and travel velocities of the porosity waves are lower compared to the case in Fig. 5a. We can also compare Figures 5b and 5c, where the values of W are similar, but the rock type differs. The comparison shows that there is more melt produced in the "metagranite" than in the "metapelite" for a similar value of W_0 due to their different solidus curves.

The models in Figures 5d and 5e show the effect of spatially variable initial water content. The model in Fig. 5d is the same as the reference case, but it includes a layer having increased initial water content, $W_{0,\mathrm{anom}} = 2.3$, which produces a higher melt fraction than its surroundings. The melt quickly percolates upward, forming a porosity wave. After 5–10 Myr, this initially anomalous layer completely disappears; the final distribution of W has a similar character as in the reference model. Fig. 5e shows the opposite case with a layer having a decreased initial water content, $W_{0,\mathrm{anom}} = 1.7$. The reduction of W has more persistent effects: even if there is a lot of melt produced below this "drier" layer, it cannot efficiently penetrate it. Instead, it accumulates just beneath it. In summary, while water-enriched anomalies move and change shapes easily, water-depleted anomalies are more stable and may represent obstacles for the melt flow.

https://doi.org/10.5194/egusphere-2026-4958
Preprint. Discussion started: 3 September 2026

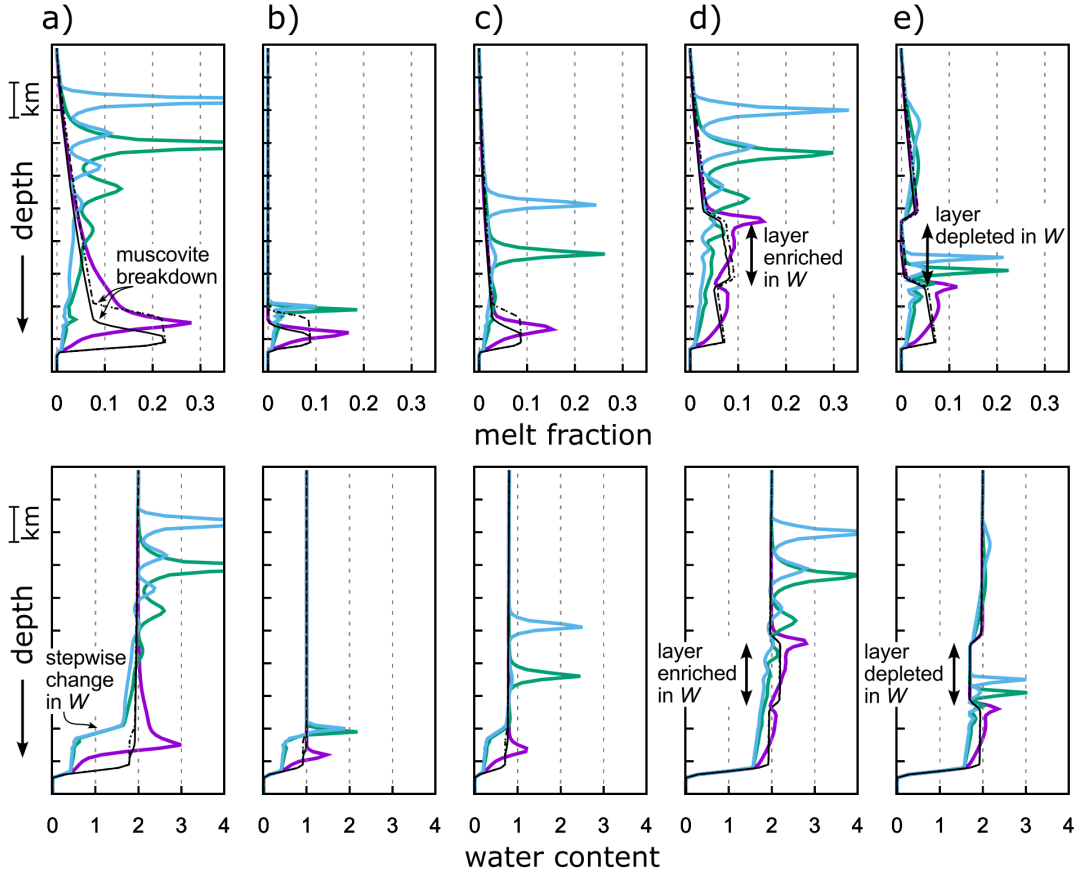

Figure 5. Effect of melt productivity. Model a) is the same as the reference model in Fig. 3 ("metapelite" rock type, $W_0 = 2$) except for a slightly warmer geotherm, which causes crossing of the muscovite breakdown within the model domain. Model b) is further modified by a decreased initial water content, $W_0 = 1$ implying zero melt productivity prior to muscovite breakdown. Model c) has "metagranite" rock type and $W_0 = 0.8$. Pressure-temperature conditions in cases a)-c) are the same: $T_{\mathrm{top}} = 650^{\circ}\mathrm{C}$, $T_{\mathrm{bot}} = 810^{\circ}\mathrm{C}$, $P_{\mathrm{top}} = 1\,\mathrm{GPa}$. Parameters in the melting law for "metapelite" and "metagranite" are the same as in Fig. 2. Pressure-temperature conditions in cases d) and e) are the same as in the reference model: $T_{\mathrm{top}} = 650^{\circ}\mathrm{C}$, $T_{\mathrm{bot}} = 790^{\circ}\mathrm{C}$, $P_{\mathrm{top}} = 1\,\mathrm{GPa}$, "metapelite" rock type and W_0=2, except for an added layer having d) increased initial $W_0 = 2.3$ and e) decreased initial $W_0 = 1.7$. Upper panels show variations of melt fraction ϕ, lower panels show variations of W. Purple, green and blue lines show the results at 1, 5 and 10 Myr of model evolution. Solid, dashed and dotted black lines show the results at 1, 5 and 10 Myr if melt percolation through the solid is switched off.

https://doi.org/10.5194/egusphere-2026-4958
Preprint. Discussion started: 3 September 2026

4.3 Effect of pressure

We investigate the effect of pressure on the efficiency of melt percolation and related changes in water content. The pressure affects the melt flow indirectly through the melt viscosity η_f. The melt viscosity depends explicitly on temperature and water content in the melt (Eq. (10)), which in turn depends on pressure and temperature as it follows the liquidus curve (Fig. 1a,b). While the temperature dependences of η_f and W_f effectively cancel out (see also nearly constant η_f in Fig. 4), the pressure dependence of W_f remains important. This is because the higher the pressure, the higher is the H_2O content of the melt. As a result, the melt viscosity decreases with pressure, which enhances melt percolation through the solid.

To demonstrate the importance of the pressure dependence of η_f, we compare three model cases that represent the same rock type and water content, but have different P–T conditions (Fig. 5). The pressure $P_{\rm top}$ is 0.5, 1 and 1.5 GPa in the three cases, respectively. In each case, the temperatures $T_{\rm top}$ and $T_{\rm bot}$ were selected so as to obtain a similar amount of melt produced in the modeled column (compare similar predicted melt fractions without melt percolation, black lines in Fig. 5abc, top row of panels). While the amount of melt is similar in these three cases, the ability of melt to percolate differs significantly.

Figure 6a shows the case with $P_{\rm top} = 0.5\,$GPa and temperature 650–720 °C. For these conditions, η_f is $\sim 10^{4.5}\,$Pa s, the melt flow is sluggish with percolation velocity of $\sim 0.3\,$mm yr^{-1}, the melt fraction evolves only slightly with time and water content is practically constant. In contrast, for $P_{\rm top} = 1\,$GPa, T=650–790 °C (Fig. 6b), η_f is $\sim 10^{4}\,$Pa s, the melt efficiently leaves the deep levels of the domain and gathers at shallow levels, which induces important variations in W. This trend is further enhanced for $P_{\rm top} = 1.5\,$GPa, T=700–850 °C (Fig. 6c) with the resulting $\eta_f \sim 10^{3.5}\,$Pa s. In this case, it is not only the high pressure, but also the high temperature that contributes to the decrease of η_f. The maximum melt percolation velocity is $\sim 1.5\,$mm yr^{-1}, that is five times higher than in the case with $P_{\rm top} = 0.5\,$GPa. The distance that the melt travels during the 10 Myrs of the model evolution is then limited mainly by the extent of the partially molten region, i.e., by the position of the solidus.

https://doi.org/10.5194/egusphere-2026-4958
Preprint. Discussion started: 3 September 2026

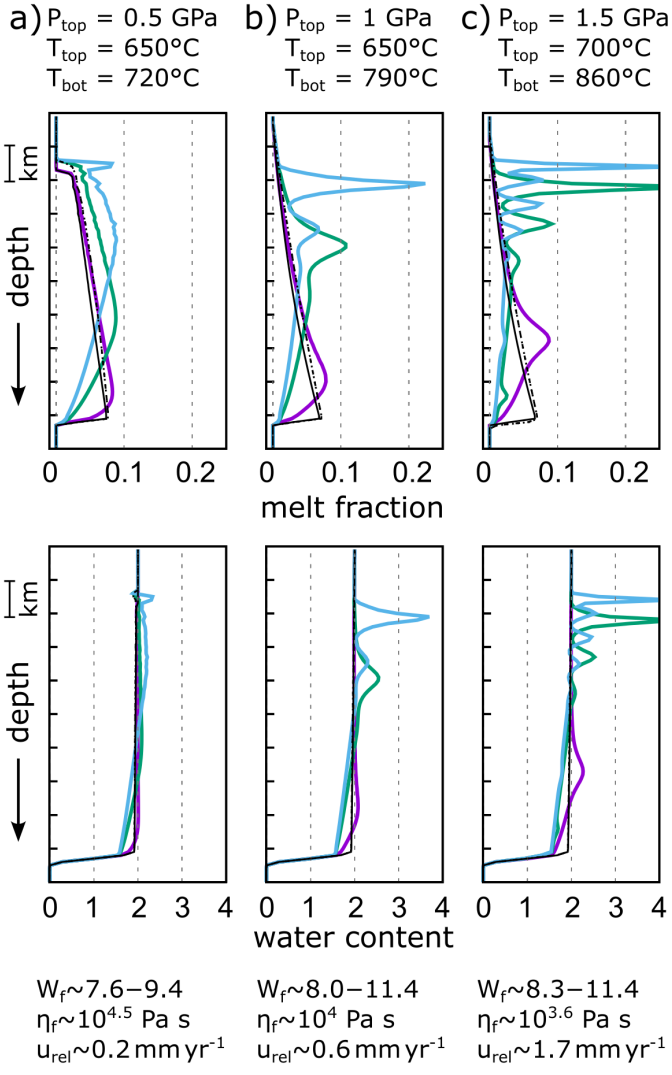

Figure 6. Effect of pressure. Results for three cases that differ in P–T conditions ($P_{\rm top}$, $T_{\rm top}$ and $T_{\rm bot}$ values noted in the figure). Parameters in the melting law are those of "metapelite" (Fig. 2); $W_0 = 2$. Values of $T_{\rm top}$ and $T_{\rm bot}$ are selected to produce similar melt amounts in the three contrasting pressure conditions, as indicated by the solid black lines in the upper panels a) to c). Upper panels show variations of melt fraction ϕ, lower panels show variations of W. Purple, green and blue lines show the results at 1, 5 and 10 Myr of model evolution. Solid, dashed and dotted black lines show the results at 1, 5 and 10 Myr if melt percolation through the solid is switched off. Beneath the panels, typical values of water content in melt (W_f), melt viscosity (η_f) and maximum relative velocity between the melt and the solid ($u_{\rm rel}$) computed in the partially molten region are noted.

https://doi.org/10.5194/egusphere-2026-4958
Preprint. Discussion started: 3 September 2026

5 Discussion

In Section 2, we defined a parameterization of melting in silica-rich rocks; limitations of this parametrization were summarized in Section 2.1. In Sections 3 and 4, we defined and described models of porous melt flow through continental crust that use this parametrization. Due to their simplicity, these models represent only the first step in this direction. Their most important limitations are the one-dimensional character and simplifications of material properties, namely rock density, rheology, permeability and melt viscosity, as summarized in Section 3.3. In the following sections, we introduce the problematics of the porous melt flow record in rocks and then compare the predictions of our models with observations of silica-rich rocks. Respecting the approximate character of the models, we focus on qualitative relationships and trends, and not on quantitative predictions.

5.1 Natural record of porous melt flow in the crust

It is widely accepted that in partially molten rocks, melt moves through the solid. In migmatites (formerly partially molten rocks), traces of melt transport are common (e.g., Brown et al., 2011; Weinberg et al., 2021), documenting that the melt transport occurs via various mechanisms. Two main situations are classically distinguished depending mainly on the ratio of crystals and melt: when rock has a rigid skeleton of crystals ("mush"), and when crystals are floating in melt (suspension, magma) (see review by Weinberg et al. (2021)). Our models are designed to mimic the cases where porous melt flow through the rigid skeleton of crystals was dominant, as opposed to the transport of magma through macroscopic conduits.

Visually, typical migmatites show bands with two contrasting parts: light-coloured leucosome and dark-coloured melanosome, interpreted as the result of melt segregation producing locally higher vs. lower melt fractions. The formation of leucosomes is related to increased melt fraction, but their exact origin remains the subject of ongoing discussion. In some studies, leucosome is used as a synonym for crystallized melt (e.g., Sawyer, 2001). Other interpretations assume that it contains crystallized melt plus residuum after melting (solid products of melting reactions) and cumulate (minerals that crystallized during melt migration) (e.g., Taylor et al., 2014). This would imply that the melt in the leucosome resided in pores in a solid crystal skeleton and moved through the pores, making two-phase flow models applicable. Indeed, the impact of porous melt flow through leucosomes was discussed in several cases (e.g., Weinberg et al., 2021; Brown et al., 2011; Slagstad et al., 2005).

A more favorable situation for the identification of porous flow is in migmatitic granites, where previous solid-state deformation produced monomineralic bands of K-feldspar, quartz and plagioclase. The crystallization of foreign mineral phases along grain boundaries within these formerly monomineralic bands is taken as evidence for passing melt (e.g., Hasalová et al., 2008b). This process homogenizes the mineral distribution without producing apparent leucosomes. Porous melt flow was identified in such granitic migmatites from thickened continental crust in the Bohemian Massif and Vosges in the European Variscides (e.g., Hasalová et al., 2008b, a; Schulmann et al., 2008; Chopin et al., 2012; Hasalová et al., 2015; Štípská et al., 2019; Aguilar et al., 2020; Závada et al., 2021, 2018). Porous melt flow without formation of distinct leucosomes was also described in intermediate-mafic rocks of arc lower crust, in Fiordland, New Zealand (e.g., Stuart et al., 2016; Chatterjee et al., 2024) and in Central Qilian Belt, NE Tibet (Sun et al., 2025).

https://doi.org/10.5194/egusphere-2026-4958
Preprint. Discussion started: 3 September 2026

Identifying and quantifying melt in silica-rich rocks remains challenging because its crystallization products—quartz, K-feldspar, and plagioclase—are mineralogically identical to the phases already present in the rock or produced during melting and melt migration. The resulting scarcity of quantitative geological data on porous melt flow ultimately limits comparison with numerical models.

5.2 Spatial and time scales

One of the key parameters that determines the importance of porous melt flow is the duration and spatial extent of supra-solidus conditions. Our models predict that at a time scale of 10 Myr, melt percolation and related changes in the water content can affect a ∼10 km thick crustal layer. Given the uncertainties in permeability (and melt viscosity), the modelled melt velocity and therefore the length scale of the affected domain may vary substantially, as predicted by the Darcy law (Eq. (6)) (e.g., McKenzie, 1984). The impact of permeability on the efficiency of the porous flow was thoroughly investigated in previous numerical studies (Jackson et al., 2003; Schmeling et al., 2019; Maierová et al., 2023). Regardless of the exact values of the parameters, both the theoretical considerations and numerical models predict that melt flow through pores along grain boundaries is a slow process. The duration of the supra-solidus conditions is, therefore, an important factor that can extend (or restrict) the region affected by melt percolation. Effects at outcrop scale (meters) can occur relatively quickly (thousands of years may be sufficient), but water-content changes at the scale of kilometers, as modelled here, may require ten(s) of millions of years. Thus, porous melt flow is expected to be important in tectonic settings where the high-temperature conditions last for extended periods. This is the case of the thickened crust in the European Variscan orogen (Štípská et al., 2016) and in the Grenville orogen (Slagstad et al., 2004), where porous melt flow was identified (see references above). In the Variscides, the duration of partial melting was estimated to ∼15 Myr; in the Grenville orogen, the melting lasted several tens of million years (e.g., Slagstad et al., 2005; Corrie and Kohn, 2008).

More generally, there is growing evidence for vertically extensive (up to tens of kilometers) partially molten zones in the continental crust (e.g., Brown et al., 2011; Wei et al., 2001). A long duration (up to tens of millions of years) of such zones has been inferred based on geochronology (Korhonen et al., 2013; Cavalcante et al., 2018; Závada et al., 2021). Previous modelling studies have shown that the SiO_2-dominated reactive flow can redistribute melt and chemical components within these zones at the vertical scale of kilometers in a few million years (e.g., Jackson et al., 2018). Our models suggest similar spatial and temporal scales for the H_2O-dominated reactive melt flow; again, we emphasize the large uncertainty of the permeability value that affects these results.

5.3 Melt flow, water content and their feedback

In models with a uniform water content, without melt flow, the melt fraction increases downward due to the temperature gradient (e.g., Fig. 4, black line). Slow ($\sim$mm yr^{-1}) melt flow through the solid is enough to entirely invert the situation. A low (but non-zero) melt fraction is then maintained in the deeper levels of the modelled rock column, and a higher melt fraction is found at shallower levels, mainly in the uppermost part of the partially molten region. Despite the 1D character of the model, the melt distribution is not simple. As the physical theory and models predict, the melt focuses and travels in waves (e.g.,

https://doi.org/10.5194/egusphere-2026-4958
Preprint. Discussion started: 3 September 2026

Spiegelman, 1993). These waves result from the positive feedback between the porosity and the speed of melt flow (see Eq. (6) and (11)); regions with increased porosity tend to drain even more melt from their surroundings, leading to a macroscopic wave-train pattern.

The development of porosity waves and high-porosity layers on top of relatively low-porosity ($<\sim$10% melt) regions is a typical result in numerical models of the reactive melt flow. The high-porosity regions develop easily especially in 1D models with impermeable bottom boundaries (e.g., Jackson et al., 2018; Solano et al., 2014), in contrast to 2D models where the advection of the partially molten material towards the cold upper boundary can result in more efficient cooling and lower melt fractions (e.g., Schmeling et al., 2019; Maierová et al., 2023). In our models, the melt tendency to accumulate in narrow zones may lead to insufficient spatial resolution (see Supplementary Material, Fig. S12).

In the rock record, the situation where melt produced at a greater depth (and higher temperature) moved via pervasive porous melt flow into a shallower level was described in the lower crust of the Variscan Bohemian Massif by Štípská et al. (2019). Based on petrography and thermodynamic modelling, these authors demonstrated that the melt inflow caused increased H_2O content in the rock thus increasing its equilibrium melt content. This feedback is somewhat obscured in the rocks: the current content of hydrous minerals does not correspond to the H_2O content during melting, because a part of H_2O was released as fluid water during solidification.

5.4 Effects of rock type, water content and its heterogeneity

With our parameterization, we approximate the difference between metagranitoids and metapelitic rocks by their typical water content bound in hydrous minerals (that define parameters $w_{1,2,3}$). The most significant difference between the two rock types is the lower melt fraction produced by metagranite compared to metapelite, caused by the lower mica content in metagranitic rocks (Fig. 2). Despite this difference, the overall melt distribution in the models is quite similar, except for the domains with maximum melt fraction, which in the "metapelite" easily surpasses 20% (compare Fig. 5a and 5c). With increasing temperature, this trend would continue; in reality, the high melt productivity of metapelites may easily cause the formation of magmatic pockets or larger bodies.

The models predict that detailed features of melt productivity, like its abrupt increase due to the muscovite breakdown, can have a profound impact on the water content. High melt productivity at depth (due to the crossing of the muscovite breakdown reaction) can cause a release of substantial melt volume which then percolates upward. This melt loss results in an important change in the water content in the source, creating a step in W at the depth of the muscovite breakdown (Fig. 5a). In other words, models predict a decrease of water content in originally fertile levels where the muscovite breakdown occurs. This can be compared, for example, with nearly dry mineralogy with garnet and kyanite in metagranites after melt loss (Lexa et al., 2011). Comparison of such compositional steps in neighboring muscovite-present and muscovite-free rocks may be a testing case for verification of our model predictions.

To assess the role of the heterogeneous water content of the rock, we modelled a case with a layer having an increased water content and therefore a higher melt productivity compared to the background (Fig. 5d). The model predicts that the initial anomalous water content is rapidly lowered due to the melt loss and efficiently homogenized with the background. In

https://doi.org/10.5194/egusphere-2026-4958
Preprint. Discussion started: 3 September 2026

natural rocks, while the amount of water in the source rock may be homogenized, other chemical components may become more heterogeneous due to the melt loss. In some cases, such compositional heterogeneities allow estimation of the melt loss, as explored by Stepanov et al. (2025).

The heterogeneity in the water content also affects the efficiency of melt flow. A zone with a low water content inhibits melt migration (Fig. 5e) because of the low melt fraction and therefore low permeability. In the 1D models, such a low-permeability obstacle cannot be surpassed and the melt remains trapped beneath it. Presumably, this could change in a 2D/3D situation, where melt can find a way around such obstacles and develop channels, possibly increasing the effective permeability of the system (c.f. Katz and Weatherley, 2012). Specifically, the typical banded structure of migmatites may facilitate or impede the melt flow, depending on the dominant inclination of the bands with respect to the pressure gradient that drives the flow (i.e., generally gravity). The interplay between the banded structure of rocks, their deformation and permeability shall be a subject for future research.

5.5 Effect of pressure

Experiments and thermodynamic models show that water content in melt increases with pressure, causing a decrease in melt viscosity (see Fig. 3), implying that the melt migrates more readily at higher pressures. Our models account for these effects on the melt viscosity and show that the porous melt flow may be significant in deep crustal levels. At pressures above ∼1 GPa, the melt flow may be efficient already at ∼5–10% melt fraction (Fig. 6b,c). At shallower crustal levels, the melt viscosity is higher and melt flow efficiency drops substantially (Fig. 6a). To our knowledge, while the pressure dependence of the water content in melt is well documented and its impact on the melt viscosity has been discussed previously (e.g., Holtz et al., 2001), no study has addressed potential implications for melt transport efficiency.

The high efficiency of porous melt flow at high pressures agrees with natural observations that describe it in the Variscan deep subduction wedge and lower crustal domes in the Bohemian Massif (Závada et al., 2018; Štípská et al., 2019; Aguilar et al., 2020) and in the arc lower crust in Fiordland (e.g., Stuart et al., 2016; Chatterjee et al., 2024). However, porous melt flow was also documented for medium-pressure conditions of 0.4–0.8 GPa in the orogenic middle crust in the Variscides (Hasalová et al., 2008b). From the perspective of our model, this pressure is too low for efficient melt percolation. However, in the Variscides, preceding phases of evolution were documented, where the partially molten rocks resided at a higher pressure (Cooke and O'Brien, 2001). Therefore, the melt flow could have taken place during an earlier phase of evolution at higher pressure, and the resulting compositional variations would then have been passively transported to lower pressure along with the bulk rock.

In the European Variscides, silica-rich rocks with very low water content, called felsic granulites, occur (e.g., Cooke and O'Brien, 2001) that have been interpreted as residues after melt loss under high-pressure conditions (>1.5 GPa) (Franěk et al., 2011; Lexa et al., 2011). These rocks typically do not contain macro-scale melt conduits (Franěk et al., 2011); instead, melt was distributed along grain boundaries, indicating porous flow as the dominant mechanism of melt transport and removal (Závada et al., 2018). While the felsic granulites are relatively rare at the surface, it has been suggested that they form a substantial portion of the Variscan lower crust (Moyen et al., 2025). Based on our models, we speculate that due to the decrease of melt

https://doi.org/10.5194/egusphere-2026-4958
Preprint. Discussion started: 3 September 2026

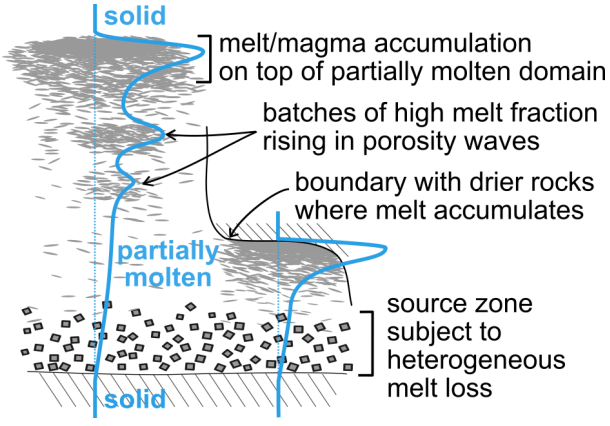

Figure 7. Sketch of a partially molten domain where the porous melt flow is efficient, together with typical variations of melt fraction (blue lines) based on our models. The melt moves from the source zone, leaving behind dry residuum. It rises in the form of porosity waves and accumulates in batches on top of the partially molten domain. The top of the partially molten domain is defined either by the solidus temperature corresponding to the water content altered by the melt inflow (i.e., more H_2O-rich compared to the initial state) or by a boundary with drier rocks that resist melting. Along its ascent path, the melt modifies the water content of the rock, as well as its microstructure, but these changes may be difficult to detect.

viscosity with depth, the porous melt flow may be an efficient process leading to such "granulitization" of spatially extensive domains in deep hot crust.

Figure 7 summarizes how our models can be interpreted in terms of melt flow in deep, hot, viscously deforming continental crust. Efficient porous melt flow can lead to the formation of zones with relatively low melt fractions ($<10\%$ melt) at depth and melt-rich–magmatic bodies at shallower levels. Solidification of melt accumulations can lead to heterogeneity in the water content. The melt can also accumulate beneath regions with low melt productivity, such as dry rocks, which act as barriers to melt flow. In the deep source region, dry rocks such as granulites that record variable melt loss dominate.

6 Concluding remarks

The parameterization of melting presented here is based on the assumption that water (H_2O component bond in hydrous minerals and free fluid phase) is the key factor determining the melt productivity of rocks. The parameterization is easily applicable in numerical models, providing a first-order estimate of melt productivity of silica-rich rocks, depending on pressure, temperature and water content.

Its applicability is demonstrated by models of gravity-driven melt flow through a crustal column. In these models, long-lasting porous melt flow typically results in a stratification with a lower melt fraction in deep levels and melt migrating as porosity waves and gathering at shallow levels of the partially molten column. This melt flow affects the water content, which then determines melt productivity — defining a feedback loop typical of the reactive melt flow. Melt extraction from the source

https://doi.org/10.5194/egusphere-2026-4958
Preprint. Discussion started: 3 September 2026

and its percolation upwards results in the drying and removal of water-content heterogeneities in the deep melt source regions. In shallow levels of the partially molten zones, variable melt inflow produces regions with an increased water content that evolves over time. In contrast, zones with a low water content, and therefore low melt productivity, behave as persistent barriers for the melt flow. Our results further suggest that pressure, rather than temperature, influences melt viscosity by requiring more water to be dissolved in the melt as pressure increases. This implies enhancement of porous melt flow in deep crustal levels, where the melt flow may be efficient already at ∼5–10% melt fraction.

Code availability. ASPECT version 3.0.0 (Heister et al., 2017; Kronbichler et al., 2012; Bangerth et al., 2024a, b) used in these computations is freely available under the GPL v2.0 or later license through its software landing page https://geodynamics.org/resources/aspect or https://aspect.geodynamics.org and is being actively developed on GitHub and can be accessed via https://github.com/geodynamics/aspect. Additional code, input files and plotting scripts to reproduce the results are available at Zenodo, doi:10.5281/zenodo.19982017 under CC BY-NC-SA 4.0.

Author contributions. PM: Investigation, Methodology, Software, Visualization. PS: Conceptualization, Methodology. PH: Conceptualization, Funding acquisition. KS: Conceptualization, Supervision. RW: Supervision. OS: Methodology. All authors: Writing.

Competing interests. The authors declare there are no conflicts of interest for this manuscript.

Acknowledgements. This research was supported by Grant 23-07821S of the Czech Science Foundation. All simulations were performed using the ASPECT software, version 2.5.0. We thank the Computational Infrastructure for Geodynamics (geodynamics.org), which is funded by the National Science Foundation under award EAR-0949446 and EAR-1550901, for supporting the development of ASPECT. Software Gnuplot and Inkscape were used to visualize the results.

https://doi.org/10.5194/egusphere-2026-4958
Preprint. Discussion started: 3 September 2026

References

Aguilar, C., Štípská, P., Chopin, F., Schulmann, K., Pitra, P., Závada, P., Hasalová, P., and Martelat, J.-E.: Syn-deformational melt percolation through a high-pressure orthogneiss and the exhumation of a subducted continental wedge (Orlica-Śnieżnik Dome, NE Bohemian Massif), International Journal of Earth Sciences, 109, 1213–1246, https://doi.org/10.1007/s00531-020-01838-4, 2020.

Annen, C., Blundy, J. D., and Sparks, R. S. J.: The Genesis of Intermediate and Silicic Magmas in Deep Crustal Hot Zones, Journal of Petrology, 47, 505–539, https://doi.org/10.1093/petrology/egi084, 2006.

Babeyko, A. Y., Sobolev, S. V., Trumbull, R., Oncken, O., and Lavier, L.: Numerical models of crustal scale convection and partial melting beneath the Altiplano–Puna plateau, Earth and Planetary Science Letters, 199, 373–388, https://doi.org/10.1016/S0012-821X(02)00597-6, 2002.

Bangerth, W., Dannberg, J., Fraters, M., Gassmoeller, R., Glerum, A., Heister, T., Myhill, R., and Naliboff, J.: ASPECT v3.0.0, https://doi.org/10.5281/zenodo.14371679, 2024a.

Bangerth, W., Dannberg, J., Fraters, M., Gassmoeller, R., Glerum, A., Heister, T., Myhill, R., and Naliboff, J.: ASPECT: Advanced Solver for Planetary Evolution, Convection, and Tectonics, User Manual, https://doi.org/10.6084/m9.figshare.4865333, 2024b.

Bonin, B., Janoušek, V., and Moyen, J.-F.: Chemical variation, modal composition and classification of granitoids, Geological Society, London, Special Publications, 491, 9–51, https://doi.org/10.1144/SP491-2019-138, 2020.

Booth, C. A., Jackson, M. D., Sparks, R. S. J., and Rust, A. C.: Source reservoir controls on the size, frequency, and composition of large-scale volcanic eruptions, Science Advances, 10, eadd1595, https://doi.org/10.1126/sciadv.add1595, 2024.

Brown, M., Korhonen, F. J., and Siddoway, C. S.: Organizing Melt Flow through the Crust, Elements, 7, 261–266, https://doi.org/10.2113/gselements.7.4.261, 2011.

Cao, W., Kaus, B. J. P., and Paterson, S.: Intrusion of granitic magma into the continental crust facilitated by magma pulsing and dike-diapir interactions: Numerical simulations, Tectonics, 35, 1575–1594, https://doi.org/10.1002/2015TC004076, 2016.

Cavalcante, C., Hollanda, M. H., Vauchez, A., and Kawata, M.: How long can the middle crust remain partially molten during orogeny?, Geology, 46, 839–842, 2018.

Chatterjee, A., Daczko, N. R., Dey, J., and Piazolo, S.: Hydrous shear zones are sites of melt transfer in the lower arc crust: A case study from Fiordland, New Zealand, Journal of Metamorphic Geology, 42, 933–956, https://doi.org/10.1111/jmg.12788, 2024.

Chopin, F., Schulmann, K., Štípská, P., Martelat, J. E., Pitra, P., Lexa, O., and Petri, B.: Microstructural and metamorphic evolution of a high-pressure granitic orthogneiss during continental subduction (Orlica–Śnieżnik dome, Bohemian Massif), Journal of Metamorphic Geology, 30, 347–376, https://doi.org/10.1111/j.1525-1314.2011.00970.x, 2012.

Clemens, J. and Vielzeuf, D.: Constraints on melting and magma production in the crust, Earth and Planetary Science Letters, 86, 287–306, https://doi.org/10.1016/0012-821X(87)90227-5, 1987.

Cooke, R. A. and O'Brien, P. J.: Resolving the relationship between high P–T rocks and gneisses in collisional terranes: an example from the Gföhl gneiss–granulite association in the Moldanubian Zone, Austria, Lithos, 58, 33–54, 2001.

Corrie, S. L. and Kohn, M. J.: Trace-element distributions in silicates during prograde metamorphic reactions: implications for monazite formation, 26, 451–464, https://doi.org/10.1111/j.1525-1314.2008.00769.x, 2008.

Costa, A., Caricchi, L., and Bagdassarov, N.: A model for the rheology of particle-bearing suspensions and partially molten rocks, Geochemistry, Geophysics, Geosystems, 10, https://doi.org/10.1029/2008GC002138, 2009.

https://doi.org/10.5194/egusphere-2026-4958
Preprint. Discussion started: 3 September 2026

Dannberg, J. and Heister, T.: Compressible magma/mantle dynamics: 3-D, adaptive simulations in ASPECT, Geophysical Journal International, 207, 1343–1366, https://doi.org/10.1093/gji/ggw329, 2016.

Dannberg, J., Gassmöller, R., Grove, R., and Heister, T.: A new formulation for coupled magma/mantle dynamics, Geophysical Journal International, 219, 94–107, 2019.

Forshaw, J. B. and Pattison, D. R.: Major-element geochemistry of pelites, Geology, 51, 39–43, https://doi.org/10.1130/G50542.1, 2023.

Franěk, J., Schulmann, K., Lexa, O., Ulrich, S., Štípská, P., Haloda, J., and Týcová, P.: Origin of felsic granulite microstructure by heterogeneous decomposition of alkali feldspar and extreme weakening of orogenic lower crust during the Variscan orogeny, 29, 103–130, https://doi.org/10.1111/j.1525-1314.2010.00911.x, 2011.

Gardien, V., Thompson, A. B., Grujic, D., and Ulmer, P.: Experimental melting of biotite + plagioclase + quartz ± muscovite assemblages and implications for crustal melting, Journal of Geophysical Research: Solid Earth, 100, 15 581–15 591, https://doi.org/10.1029/95JB00916, 1995.

Giordano, D., Russell, J. K., and Dingwell, D. B.: Viscosity of magmatic liquids: A model, Earth and Planetary Science Letters, 271, 123–134, https://doi.org/10.1016/j.epsl.2008.03.038, 2008.

Gorczyk, W. and Vogt, K.: Intrusion of Magmatic Bodies Into the Continental Crust: 3-D Numerical Models, Tectonics, 37, 705–723, https://doi.org/10.1002/2017TC004738, 2018.

Green, E. C. R., Holland, T. J. B., Powell, R., Weller, O. M., and Riel, N.: Corrigendum to: Melting of Peridotites through to Granites: a Simple Thermodynamic Model in the System KNCFMASHTOCr, and, a Thermodynamic Model for the Subsolidus Evolution and Melting of Peridotite. | Journal of Petrology | Oxford Academic, 66, https://doi.org/https://doi.org/10.1093/petrology/egae079, 2025.

Hasalová, P., Schulmann, K., Lexa, O., Štípská, P., Hrouda, F., Ulrich, S., Haloda, J., and Týcová, P.: Origin of migmatites by deformation-enhanced melt infiltration of orthogneiss: a new model based on quantitative microstructural analysis, Journal of Metamorphic Geology, 26, 29–53, https://doi.org/10.1111/j.1525-1314.2007.00743.x, 2008a.

Hasalová, P., Štípská, P., Powell, R., Schulmann, K., Janoušek, V., and Lexa, O.: Transforming mylonitic metagranite by open-system interactions during melt flow, Journal of Metamorphic Geology, 26, 55–80, https://doi.org/10.1111/j.1525-1314.2007.00744.x, 2008b.

Hasalová, P., Schulmann, K., Tabaud, A. S., and Oliot, E.: Microstructural evidences for mineralogical inheritance in partially molten rocks: example from the Vosges Mts, Bulletin de la Société Géologique de France, 186, 131–143, 2015.

Heister, T., Dannberg, J., Gassmöller, R., and Bangerth, W.: High Accuracy Mantle Convection Simulation through Modern Numerical Methods. II: Realistic Models and Problems, Geophysical Journal International, 210, 833–851, https://doi.org/10.1093/gji/ggx195, 2017.

Hess, K.-U. and Dingwell, D. D.: Viscosities of hydrous leucogranitic melts: A non-Arrhenian model, American Mineralogist, 81, 1297–1300, 1996.

Holland, T. J. B. and Powell, R.: Calculation of Phase Relations Involving Haplogranitic Melts Using an Internally Consistent Thermodynamic Dataset, Journal of Petrology, 42, 673–683, https://doi.org/10.1093/petrology/42.4.673, 2001.

Holland, T. J. B., Green, E. C. R., and Powell, R.: Melting of Peridotites through to Granites: A Simple Thermodynamic Model in the System KNCFMASHTOCr, Journal of Petrology, 59, 881–900, https://doi.org/10.1093/petrology/egy048, 2018.

Holtz, F., Johannes, W., Tamic, N., and Behrens, H.: Maximum and minimum water contents of granitic melts generated in the crust: a reevaluation and implications, Lithos, 56, 1–14, 2001.

Hu, H., Jackson, M. D., and Blundy, J.: Melting, Compaction and Reactive Flow: Controls on Melt Fraction and Composition Change in Crustal Mush Reservoirs, Journal of Petrology, 63, egac097, https://doi.org/10.1093/petrology/egac097, 2022.

https://doi.org/10.5194/egusphere-2026-4958
Preprint. Discussion started: 3 September 2026

Jackson, M. D., Cheadle, M. J., and Atherton, M. P.: Quantitative modeling of granitic melt generation and segregation in the continental crust, 108, https://doi.org/10.1029/2001JB001050, 2003.

Jackson, M. D., Blundy, J., and Sparks, R. S. J.: Chemical differentiation, cold storage and remobilization of magma in the Earth's crust, Nature, 564, 405–409, https://doi.org/10.1038/s41586-018-0746-2, 2018.

Jamieson, R. A., Unsworth, M. J., Harris, N. B., Rosenberg, C. L., and Schulmann, K.: Crustal melting and the flow of mountains, Elements, 7, 253–260, 2011.

Johannes, W. and Holtz, F.: Petrogenesis and experimental petrology of granitic rocks, Springer-Verlag, Berlin, 1996.

Katz, R. F. and Weatherley, S. M.: Consequences of mantle heterogeneity for melt extraction at mid-ocean ridges, Earth and Planetary Science Letters, 335-336, 226–237, https://doi.org/10.1016/j.epsl.2012.04.042, 2012.

Katz, R. F., Spiegelman, M., and Langmuir, C. H.: A new parameterization of hydrous mantle melting, Geochemistry, Geophysics, Geosystems, 4, 2002GC000 433, https://doi.org/10.1029/2002GC000433, 2003.

Katz, R. F., Jones, D. W. R., Rudge, J. F., and Keller, T.: Physics of Melt Extraction from the Mantle: Speed and Style, Annual Review of Earth and Planetary Sciences, 50, 507–540, https://doi.org/10.1146/annurev-earth-032320-083704, 2022.

Keller, T. and Katz, R. F.: The Role of Volatiles in Reactive Melt Transport in the Asthenosphere, Journal of Petrology, 57, 1073–1108, https://doi.org/10.1093/petrology/egw030, 2016.

Keller, T., May, D. A., and Kaus, B. J.: Numerical modelling of magma dynamics coupled to tectonic deformation of lithosphere and crust, Geophysical Journal International, 195, 1406–1442, 2013.

Kerswell, B., Cerpa, N. G., Tommasi, A., Godard, M., and Padrón-Navarta, J. A.: RocMLMs: Predicting Rock Properties Through Machine Learning Models, Journal of Geophysical Research: Machine Learning and Computation, 1, e2024JH000 264, https://doi.org/10.1029/2024JH000264, 2024.

Korhonen, F. J., Clark, C., Brown, M., Bhattacharya, S., and Taylor, R.: How long-lived is ultrahigh temperature (UHT) metamorphism? Constraints from zircon and monazite geochronology in the Eastern Ghats orogenic belt, India, Precambrian Research, 234, 322–350, https://doi.org/10.1016/j.precamres.2012.12.001, 2013.

Kronbichler, M., Heister, T., and Bangerth, W.: High Accuracy Mantle Convection Simulation through Modern Numerical Methods, Geophysical Journal International, 191, 12–29, https://doi.org/10.1111/j.1365-246X.2012.05609.x, 2012.

Lexa, O., Schulmann, K., Janoušek, V., Štípská, P., Guy, A., and Racek, M.: Heat sources and trigger mechanisms of exhumation of HP granulites in Variscan orogenic root, Journal of Metamorphic Geology, 29, 79–102, https://doi.org/10.1111/j.1525-1314.2010.00906.x, 2011.

Li, Y., Pusok, A. E., Davis, T., May, D. A., and Katz, R. F.: Continuum approximation of dyking with a theory for poro-viscoelastic–viscoplastic deformation, Geophysical Journal International, 234, 2007–2031, https://doi.org/10.1093/gji/ggad173, 2023.

Louis-Napoléon, A., Gerbault, M., Bonometti, T., Vanderhaeghe, O., Martin, R., and Maury, N.: Convection and segregation in heterogeneous orogenic crust with a VOF method – II: how to form migmatite domes, Geophysical Journal International, 236, 207–232, https://doi.org/10.1093/gji/ggad388, 2024.

Maierová, P., Hasalová, P., Schulmann, K., Štípská, P., and Souček, O.: Porous Melt Flow in Continental Crust—A Numerical Modeling Study, Journal of Geophysical Research: Solid Earth, 128, e2023JB026 523, https://doi.org/10.1029/2023JB026523, 2023.

Makhluf, A. R., Newton, R. C., and Manning, C. E.: Experimental determination of liquidus H2O contents of haplogranite at deep-crustal conditions, Contributions to Mineralogy and Petrology, 172, 77, https://doi.org/10.1007/s00410-017-1392-7, 2017.

McKenzie, D.: The generation and compaction of partially molten rock, Journal of Petrology, 25, 713–765, 1984.

https://doi.org/10.5194/egusphere-2026-4958
Preprint. Discussion started: 3 September 2026

Moyen, J.-F., Guy, A., Fiannacca, P., Janoušek, V., Villaseca, C., and Arribas, P. A.: Granites and the Nature of the Variscan Crust, Elements, 21, 415–421, https://doi.org/10.2138/gselements.21.6.415, 2025.

Pavan, M., Sawyer, E. W., Moraes, R., and Faleiros, F. M.: Partial melting of granodiorite: insights from ediacaran granulite-facies metamorphism in Southern Brazil, Journal of Petrology, 62, egab028, https://doi.org/10.1093/petrology/egab028, 2021.

Petford, N., Lister, J. R., and Kerr, R. C.: The ascent of felsic magmas in dykes, Lithos, 32, 161–168, https://doi.org/10.1016/0024-4937(94)90028-0, 1994.

Plunder, A., Le Pourhiet, L., Räss, L., Gloaguen, E., Pichavant, M., and Gumiaux, C.: Pegmatites as geological expressions of spontaneous crustal flow localisation, Lithos, 416-417, 106 652, https://doi.org/10.1016/j.lithos.2022.106652, 2022.

Renner, J., Evans, B., and Hirth, G.: On the rheologically critical melt fraction, Earth and Planetary Science Letters, 181, 585–594, https://doi.org/10.1016/S0012-821X(00)00222-3, 2000.

Riel, N., Kaus, B. J. P., Green, E. C. R., and Berlie, N.: MAGEMin, an Efficient Gibbs Energy Minimizer: Application to Igneous Systems, Geochemistry, Geophysics, Geosystems, 23, e2022GC010 427, https://doi.org/10.1029/2022GC010427, 2022.

Rudge, J. F.: The viscosities of partially molten materials undergoing diffusion creep, Journal of Geophysical Research: Solid Earth, 123, 10–534, 2018.

Rummel, L., Kaus, B. J. P., Baumann, T. S., White, R. W., and Riel, N.: Insights into the Compositional Evolution of Crustal Magmatic Systems from Coupled Petrological-Geodynamical Models, Journal of Petrology, 61, egaa029, https://doi.org/10.1093/petrology/egaa029, 2020.

Sawyer, E. W.: Melt segregation in the continental crust: distribution and movement of melt in anatectic rocks, Journal of Metamorphic Geology, 19, 291–309, 2001.

Sawyer, E. W., Cesare, B., and Brown, M.: When the continental crust melts, Elements, 7, 229–234, 2011.

Schmeling, H., Kruse, J. P., and Richard, G.: Effective shear and bulk viscosity of partially molten rock based on elastic moduli theory of a fluid filled poroelastic medium, Geophysical Journal International, 190, 1571–1578, https://doi.org/10.1111/j.1365-246X.2012.05596.x, 2012.

Schmeling, H., Marquart, G., Weinberg, R., and Wallner, H.: Modelling melting and melt segregation by two-phase flow: new insights into the dynamics of magmatic systems in the continental crust, Geophysical Journal International, 217, 422–450, https://doi.org/10.1093/gji/ggz029, 2019.

Schmeling, H., Marquart, G., Weinberg, R., and Kumaravel, P.: Dynamic two-phase flow modelling of melt segregation in continental crust: batholith emplacement vs. crustal convection, with implications for magmatism in thickened plateaus, Geochemistry, Geophysics, Geosystems, p. IN PRESS, 2023.

Schulmann, K., Martelat, J.-E., Ulrich, S., Lexa, O., Štípská, P., and Becker, J. K.: Evolution of microstructure and melt topology in partially molten granitic mylonite: Implications for rheology of felsic middle crust, Journal of Geophysical Research: Solid Earth, 113, 2008.

Schulze, F., Behrens, H., Holtz, F., Roux, J., and Johannes, W.: The influence of H2O on the viscosity of a haplogranitic melt, American Mineralogist, 81, 1155–1165, 1996.

Simpson, G., Spiegelman, M., and Weinstein, M. I.: A multiscale model of partial melts: 1. Effective equations, Journal of Geophysical Research: Solid Earth, 115, 2009JB006 375, https://doi.org/10.1029/2009JB006375, 2010.

Slagstad, T., Hamilton, M. A., Jamieson, R. A., and Culshaw, N. G.: Timing and duration of melting in the mid orogenic crust: Constraints from UPb (SHRIMP) data, Muskoka and Shawanaga domains, Grenville Province, Ontario, Canadian Journal of Earth Sciences, 41, 1339–1365, https://doi.org/10.1139/e04-068, 2004.

https://doi.org/10.5194/egusphere-2026-4958
Preprint. Discussion started: 3 September 2026

Slagstad, T., Jamieson, R. A., and Culshaw, N. G.: Formation, Crystallization, and Migration of Melt in the Mid-orogenic Crust: Muskoka Domain Migmatites, Grenville Province, Ontario, Journal of Petrology, 46, 893–919, https://doi.org/10.1093/petrology/egi004, 2005.

Solano, J., Jackson, M., Sparks, R., and Blundy, J.: Evolution of major and trace element composition during melt migration through crystalline mush: implications for chemical differentiation in the crust, American Journal of Science, 314, 895–939, 2014.

Spiegelman, M.: Flow in deformable porous media. Part 2 Numerical analysis – the relationship between shock waves and solitary waves, Journal of Fluid Mechanics, 247, 39–63, https://doi.org/10.1017/S0022112093000370, 1993.

Spiegelman, M., Katz, R., and Simpson, G.: An introduction and tutorial to the "McKenzie Equations" for magma migration, Preprint, Columbia University, Dept. of Applied Physics and Applied Mathematics, 2007.

Stepanov, A. S., Weinberg, R., Mayne, M. J., and Jiang, S.-Y.: Melt Loss Quantification from Restites of Heterogeneous Metasedimentary Protoliths Revealing Volatile Redistribution during Mid-Crustal Anatexis, Journal of Petrology, 66, egaf046, https://doi.org/10.1093/petrology/egaf046, 2025.

Stuart, C. A., Piazolo, S., and Daczko, N. R.: Mass transfer in the lower crust: Evidence for incipient melt assisted flow along grain boundaries in the deep arc granulites of Fiordland, New Zealand, Geochemistry, Geophysics, Geosystems, 17, 3733–3753, 2016.

Sun, X., Wang, C., Daczko, N. R., Liao, X., Zhang, J., Yang, W., and Liu, L.: Reactive Melt Flow in the Continental Arc Root: Insights for the Transition From Gabbronorite to Garnet Granulite in the Central Qilian Belt, NE Tibet, Geochemistry, Geophysics, Geosystems, 26, e2025GC012 366, https://doi.org/10.1029/2025GC012366, 2025.

Taylor, J., Nicoli, G., Stevens, G., Frei, D., and Moyen, J.-F.: The processes that control leucosome compositions in metasedimentary granulites: perspectives from the Southern Marginal Zone migmatites, Limpopo Belt, South Africa, Journal of Metamorphic Geology, 32, 713–742, https://doi.org/10.1111/jmg.12087, 2014.

Thompson, A. B.: Dehydration melting of pelitic rocks and the generation of H 2 O-undersaturated granitic liquids, American Journal of Science, 282, 1567–1595, https://doi.org/10.2475/ajs.282.10.1567, 1982.

Vielzeuf, D. and Schmidt, M. W.: Melting relations in hydrous systems revisited: application to metapelites, metagreywackes and metabasalts, Contributions to Mineralogy and Petrology, 141, 251–267, https://doi.org/10.1007/s004100100237, 2001.

Wei, W., Unsworth, M., Jones, A., Booker, J., Tan, H., Nelson, D., Chen, L., Li, S., Solon, K., Bedrosian, P., and others: Detection of widespread fluids in the Tibetan crust by magnetotelluric studies, Science, 292, 716–719, 2001.

Weinberg, R. F.: Mesoscale pervasive felsic magma migration: alternatives to dyking, Lithos, 46, 393–410, https://doi.org/10.1016/S0024-4937(98)00075-9, 1999.

Weinberg, R. F. and Hasalová, P.: Water-fluxed melting of the continental crust: A review, Lithos, 212, 158–188, 2015.

Weinberg, R. F. and Regenauer-Lieb, K.: Ductile fractures and magma migration from source, Geology, 38, 363–366, 2010.

Weinberg, R. F., Vernon, R. H., and Schmeling, H.: Processes in mushes and their role in the differentiation of granitic rocks, Earth-Science Reviews, 220, 103 665, 2021.

White, R. W. and Powell, R.: Melt loss and the preservation of granulite facies mineral assemblages, Journal of Metamorphic Geology, 20, 621–632, https://doi.org/10.1046/j.1525-1314.2002.00206_20_7.x, 2002.

White, R. W., Powell, R., and Holland, T. J. B.: Calculation of partial melting equilibria in the system Na $_2$ O-CaO-K $_2$ O-FeO-MgO-Al $_2$ O $_3$ -SiO $_2$ -H $_2$ O (NCKFMASH): PARTIAL MELTING EQUILIBRIA IN NCKFMASH, Journal of Metamorphic Geology, 19, 139–153, https://doi.org/10.1046/j.0263-4929.2000.00303.x, 2001.

White, R. W., Stevens, G., and Johnson, T. E.: Is the Crucible Reproducible? Reconciling Melting Experiments with Thermodynamic Calculations, Elements, 7, 241–246, https://doi.org/10.2113/gselements.7.4.241, 2011.

https://doi.org/10.5194/egusphere-2026-4958
Preprint. Discussion started: 3 September 2026

White, R. W., Powell, R., Holland, T. J. B., Johnson, T. E., and Green, E. C. R.: New mineral activity–composition relations for thermodynamic calculations in metapelitic systems, Journal of Metamorphic Geology, 32, 261–286, https://doi.org/10.1111/jmg.12071, 2014.

Whittington, A., Richet, P., Behrens, H., Holtz, F., and Scaillet, B.: Experimental temperature–X (H2O)–viscosity relationship for leucogranites and comparison with synthetic silicic liquids, Earth and Environmental Science Transactions of The Royal Society of Edinburgh, 95, 59–71, 2004.

Závada, P., Schulmann, K., Racek, M., Hasalová, P., Jeřábek, P., Weinberg, R. F., Štípská, P., and Roberts, A.: Role of strain localization and melt flow on exhumation of deeply subducted continental crust, Lithosphere, 10, 217–238, https://doi.org/10.1130/L666.1, 2018.

Závada, P., Štípská, P., Hasalová, P., Racek, M., Jeřábek, P., Schulmann, K., Kylander-Clark, A., and Holder, R.: Monazite geochronology in melt-percolated UHP meta-granitoids: an example from the Erzgebirge continental subduction wedge, Bohemian Massif, Chemical Geology, 559, 119 919, 2021.

Štípská, P., Powell, R., Hacker, B. R., Holder, R., and Kylander-Clark, A. R. C.: Uncoupled U/Pb and REE response in zircon during the transformation of eclogite to mafic and intermediate granulite (Blanský les, Bohemian Massif), Journal of Metamorphic Geology, 34, 551–572, https://doi.org/10.1111/jmg.12193, 2016.

Štípská, P., Hasalová, P., Powell, R., Závada, P., Schulmann, K., Racek, M., Aguilar, C., and Chopin, F.: The effect of melt infiltration on metagranitic rocks: The Snieznik dome, Bohemian Massif, Journal of Petrology, 60, 591–618, 2019.

https://doi.org/10.5194/egusphere-2026-4958
Preprint. Discussion started: 3 September 2026

Appendix A: Numerical model description

A1 Governing equations

We use a mathematical formulation that describes deformation of two phases — solid rock and melt (indices s and f, standing for solid and fluid, respectively). The solid and melt can deform as well as move relative to each other, and the transformation between them corresponds to melting and solidification. As there are only two material phases in the model, the volumetric fraction of the melt is equal to the volumetric fraction of pores in the matrix, which is also referred to as porosity. The formulation follows the approach of McKenzie (1984), further developed and implemented into ASPECT software by Dannberg and Heister (2016). The presented models are (pseudo-)one-dimensional and focus on melt percolation through the solid. The deformation of the solid in one dimension is highly restricted and plays a role only because it is coupled with melt flow and melting due to mass conservation.

Total mass balances for the solid and melt are expressed as:

$$\frac{\partial((1-\phi)\rho_s)}{\partial t} + \nabla\cdot((1-\phi)\rho_s\mathbf{u}_s) = -\Gamma, \tag{A1}$$

$$\frac{\partial(\phi\rho_f)}{\partial t} + \nabla\cdot(\phi\rho_f\mathbf{u}_f) = \Gamma, \tag{A2}$$

where ϕ is the porosity, $\mathbf{u}_f$ is the velocity of melt, $\mathbf{u}_s$ is the velocity of solid, ρ_f is the melt density, ρ_s is the solid density and Γ is the rate of melting. Assuming that ρ_s and ρ_f are constants, we can sum these two equations and obtain the mass balance in the two-phase material:

$$\nabla\cdot[\phi\mathbf{u}_f + (1-\phi)\mathbf{u}_s] = \Gamma\left(\frac{1}{\rho_f} - \frac{1}{\rho_s}\right). \tag{A3}$$

The conservation of momentum in the two-phase material is expressed as:

$$-\nabla\cdot(2\eta_s\dot{\boldsymbol{\epsilon}}') + \nabla p_f + \nabla p_c = \rho\mathbf{g}, \tag{A4}$$

where η_s is the solid shear viscosity, $\dot{\boldsymbol{\epsilon}}' = \dot{\boldsymbol{\epsilon}} - \frac{1}{3}(\nabla\cdot\mathbf{u}_s)\mathbf{I}$ is the deviatoric part of the solid strain rate tensor $\dot{\boldsymbol{\epsilon}} = \frac{1}{2}(\nabla\mathbf{u}_s + \nabla^{\mathrm{T}}\mathbf{u}_s)$, p_f is the melt pressure, p_c is the compaction pressure defined as:

$$p_c = -\eta_b(\nabla\cdot\mathbf{u}_s), \tag{A5}$$

where η_b is the bulk viscosity of the solid matrix, $\mathbf{g}$ is the gravity and the density ρ is calculated from the densities of the solid and melt phases:

$$\rho = (1-\phi)\rho_s + \phi\rho_f. \tag{A6}$$

The central equation in the adopted formulation is the Darcy law, which approximates the conservation of momentum of the melt. It expresses the velocity of the melt with respect to the solid, $\mathbf{u}_{\mathrm{rel}}$:

$$\mathbf{u}_{\mathrm{rel}} = \mathbf{u}_f - \mathbf{u}_s = \frac{k_\phi}{\eta_f\phi}(\rho_f\mathbf{g} - \nabla p_f), \tag{A7}$$

https://doi.org/10.5194/egusphere-2026-4958
Preprint. Discussion started: 3 September 2026

where k_ϕ is the porosity-dependent permeability and η_f is the melt viscosity. Besides the solid and melt motions, we solve the equation of heat transport, including the advection and diffusion terms and the latent heat of melting/solidification:

$$\phi\rho_f c_p\left(\frac{\partial T}{\partial t}+\mathbf{u}_f\cdot\nabla T\right)+(1-\phi)\rho_s c_p\left(\frac{\partial T}{\partial t}+\mathbf{u}_s\cdot\nabla T\right)-\nabla\cdot(k_T\nabla T)=T\Delta S\Gamma\,, \tag{A8}$$

where T is the temperature, t is time, c_p is the heat capacity, k_T is the heat conductivity (the same for the solid and melt) and ΔS is the entropy change due to melting. This equation assumes thermal equilibrium between the melt and the solid and therefore the temperature is the same in both phases.

We track the change in the porosity defined by the mass conservation of the solid (A1). It can be expressed in the form of the advection equation for the porosity, with additional right-hand-side terms representing the compaction of the solid matrix and melting:

$$\frac{\partial\phi}{\partial t}+\mathbf{u}_s\cdot\nabla\phi=(1-\phi)\nabla\cdot\mathbf{u}_s+\frac{\Gamma}{\rho_s}\,. \tag{A9}$$

Further, we track the water content in the solid (W_s) and the melt (W_f) as they are advected by their respective velocities and affected by melting:

$$\frac{\partial W_s}{\partial t}+\mathbf{u}_s\cdot\nabla W_s=\Gamma_s\,, \tag{A10}$$

$$\frac{\partial W_f}{\partial t}+\mathbf{u}_f\cdot\nabla W_f=\Gamma_f\,, \tag{A11}$$

where the reaction rates Γ_s and Γ_f are defined by the melting model (see below).

A2 Definition of W

To describe the melting process and associated changes of W_s and W_f, we first have to specify the meaning of the "composition" W. We define it as the mass fraction of a certain chemical component, X, in the partially molten material. In our melting parametrization, it is the mass fraction of H_2O, but generally it may be any chemical component of the material. W_s and W_f are then mass fractions of the component X in the solid and fluid, respectively.

Let ρ_X be the partial density of the component X (i.e., mass of the component X distributed between the melt and solid phases, per unit volume of the two-phase mixture):

$$\rho_X=\rho_f\phi W_f+\rho_s(1-\phi)W_s. \tag{A12}$$

Using (A12) and (A6), the water content W can be defined as:

$$W=\frac{\rho_X}{\rho}=\frac{\rho_f\phi W_f+\rho_s(1-\phi)W_s}{\rho_f\phi+\rho_s(1-\phi)}. \tag{A13}$$

We use the melting model described in the main text, where the melting is parametrized using the solidus and liquidus temperatures, both functions of pressure and W. From Fig. 1a in the main text it follows that the solidus and liquidus lines

https://doi.org/10.5194/egusphere-2026-4958
Preprint. Discussion started: 3 September 2026

define not only the solidus and liquidus temperatures, but also the equilibrium water contents of the solid and the melt, W_{sx} and W_{fx} (for a given temperature and pressure). The equilibrium water contents then define the equilibrium melt fraction, so that the mass of the component X is conserved.

Here it should be noted that two types of melt fraction can be defined. The first is the volumetric melt fraction, which in the case of the two-phase melt-solid material coincides with the porosity ϕ. The second is the mass melt fraction, ϕ_{mass}:

$$\phi_{\mathrm{mass}} = \frac{\rho_f \phi}{\rho_f \phi + \rho_s (1-\phi)}. \tag{A14}$$

Using (A13) in (A14) yields formula (4) in the main text. The equilibrium melt fraction can be calculated as follows: For temperatures below the solidus, the equilibrium melt fraction (both volume-based and mass-based) is zero. For temperatures above the liquidus, the material is entirely molten and the equilibrium melt fraction is 1. In between the solidus and liquidus temperatures, the equilibrium melt fraction can be expressed from (A13) and (A14) as the lever rule:

$$\phi_{\mathrm{mass}x} = \frac{W_{sx} - W}{W_{sx} - W_{fx}}. \tag{A15}$$

A3 Implementation of melting and water content equilibration

The solution of the advection equations for W_s (A10), W_f (A11), porosity (A9) and temperature (A8) is split into two steps. In the first step, we solve the advection equations for the solid and liquid water contents without the reaction terms:

$$\frac{\partial W_s|_{\mathrm{adv}}}{\partial t} + \mathbf{u}_s \cdot \nabla W_s|_{\mathrm{adv}} = 0, \tag{A16}$$

$$\frac{\partial W_f|_{\mathrm{adv}}}{\partial t} + \mathbf{u}_f \cdot \nabla W_f|_{\mathrm{adv}} = 0, \tag{A17}$$

and analogous equations for porosity (A9) and temperature (A8) without the terms containing Γ:

$$\frac{\partial \phi|_{\mathrm{adv}}}{\partial t} + \mathbf{u}_s \cdot \nabla \phi|_{\mathrm{adv}} = (1-\phi|_{\mathrm{adv}}) \nabla \cdot \mathbf{u}_s, \tag{A18}$$

$$\phi|_{\mathrm{adv}} \rho_f c_p \left(\frac{\partial T|_{\mathrm{adv}}}{\partial t} + \mathbf{u}_f \cdot \nabla T|_{\mathrm{adv}} \right) + (1-\phi|_{\mathrm{adv}}) \rho_s c_p \left(\frac{\partial T|_{\mathrm{adv}}}{\partial t} + \mathbf{u}_s \cdot \nabla T|_{\mathrm{adv}} \right) - \nabla \cdot (k_T \nabla T|_{\mathrm{adv}}) = 0. \tag{A19}$$

In the second step, the partial water contents, porosity and temperature are modified due to water content equilibration, melting and latent heat release: "reactive" updates are added to the "advective" solutions (A16)–(A19).

After the advection step, W_s and W_f in general do not lie on the solidus and liquidus lines. The "reactive" updates ΔW_s and ΔW_f are required to correct them, and the porosity update $\Delta\phi$ is required to ensure mass conservation of the component X.

Comparing (A16)–(A19) vs. (A8)–(A11) we can express the relationships between the updates and the reaction rates:

$$\Delta W_s = \Gamma_s \Delta t, \tag{A20}$$

$$\Delta W_f = \Gamma_f \Delta t, \tag{A21}$$

$$\Delta \phi = \frac{\Gamma}{\rho_s} \Delta t. \tag{A22}$$

https://doi.org/10.5194/egusphere-2026-4958
Preprint. Discussion started: 3 September 2026

(Note that this definition of $\Delta\phi$ is valid for the reaction update of (A9) that is derived from (A1), and not of an analogous equation that can be derived from (A2).)

If the temperature is **between the solidus and the liquidus**, we calculate the updates from the equilibrium partial water contents:

$$\Delta W_s = W_{sx} - W_s|_{\mathrm{adv}}\,, \tag{A23}$$
$$\Delta W_f = W_{fx} - W_f|_{\mathrm{adv}}\,.$$

To calculate the porosity update, we first determine the relationship between the reaction rates Γ_s and Γ_f and the melting reaction rate Γ. Multiplying equation (A10) by $\rho_s(1-\phi)$ and equation (A11) by $\rho_f\phi$ and summing the resulting two equations we get:

$$\frac{\partial(\rho W)}{\partial t} + \nabla\cdot\left(\rho_f\phi W_f\mathbf{u}_f + \rho_s(1-\phi)W_s\mathbf{u}_s\right) = \rho_f\phi\Gamma_f + \rho_s(1-\phi)\Gamma_s + (W_f - W_s)\,\Gamma. \tag{A24}$$

Conservation of total mass of the component X (integral of ρW is constant over any domain with impermeable boundaries) implies that integrals of both the left-hand side and the right-hand side of (A24) over such domains must be zero. Since the right-hand side represents only purely reactive terms, depending only on local thermodynamic conditions and melt fraction, one may by a localization argument infer that both sides of (A24) must be locally zero everywhere, i.e.:

$$\frac{\partial(\rho W)}{\partial t} + \nabla\cdot\left(\rho_f\phi W_f\mathbf{u}_f + \rho_s(1-\phi)W_s\mathbf{u}_s\right) = 0 \tag{A25}$$

and

$$\rho_f\phi\Gamma_f + \rho_s(1-\phi)\Gamma_s + (W_f - W_s)\Gamma = 0, \tag{A26}$$

which can be rearranged as:

$$\Gamma = \frac{\rho_f\phi\Gamma_f + \rho_s(1-\phi)\Gamma_s}{W_s - W_f}. \tag{A27}$$

The porosity update is then:

$$\Delta\phi = \frac{\Gamma}{\rho_s}\Delta t = \frac{\rho_f\phi\Gamma_f + \rho_s(1-\phi)\Gamma_s}{\rho_s(W_s - W_f)}\Delta t = \frac{\rho_f\phi\Delta W_f + \rho_s(1-\phi)\Delta W_s}{\rho_s(W_s - W_f)}\,. \tag{A28}$$

Note that W_f and W_s have to be already corrected by the reactive update (i.e., they are not the advective solutions).

If the temperature is **below the solidus** temperature, the relationships (A23) and (A28) for the updates are not applicable. If the porosity is zero in this case, there is no melt and W_s (and formally also W_f) does not change by reaction. However, a situation may occur where, after the advection step, $\phi|_{\mathrm{adv}} > 0$. In that case, the "reactions" act to reach the equilibrium porosity $\phi_x = 0$, while ensuring the conservation of mass of the component X. The porosity update is then calculated from the equilibrium porosity:

$$\Delta\phi = \phi_x - \phi|_{\mathrm{adv}} = -\phi|_{\mathrm{adv}}\,. \tag{A29}$$

https://doi.org/10.5194/egusphere-2026-4958
Preprint. Discussion started: 3 September 2026

From (A26) for $\phi = 0$ we get:

$$\rho_s \Gamma_s + (W_f - W_s)\Gamma = 0\,, \tag{A30}$$

and using $W_s|_{\mathrm{adv}}$ and $W_f|_{\mathrm{adv}}$ as predictors of W_s and W_f, respectively, the update of the solid water content is:

$$\Gamma_s = (W_s|_{\mathrm{adv}} - W_f|_{\mathrm{adv}})\frac{\Gamma}{\rho_s} = (W_s|_{\mathrm{adv}} - W_f|_{\mathrm{adv}})\frac{\Delta\phi}{\Delta t} = -(W_s|_{\mathrm{adv}} - W_f|_{\mathrm{adv}})\frac{\phi|_{\mathrm{adv}}}{\Delta t}, \tag{A31}$$

implying

$$\Delta W_s = -(W_s|_{\mathrm{adv}} - W_f|_{\mathrm{adv}})\phi|_{\mathrm{adv}}. \tag{A32}$$

The definition of ΔW_f is not straightforward, because below the solidus, there is no melt in equilibrium. However, we can define it using (A26), where we plug in (A29) and (A31), which yields:

$$\Gamma_f = -\frac{\rho_s}{\rho_f}(W_s|_{\mathrm{adv}} - W_f|_{\mathrm{adv}})\frac{\phi|_{\mathrm{adv}}}{\Delta t} \qquad \Longrightarrow \qquad \Delta W_f = -\frac{\rho_s}{\rho_f}(W_s|_{\mathrm{adv}} - W_f|_{\mathrm{adv}})\phi|_{\mathrm{adv}}. \tag{A33}$$

Analogously, for the temperature **above the liquidus** temperature, the equilibrium porosity equals 1 and the updates are:

$$\begin{aligned} \Delta\phi &= \phi_x - \phi|_{\mathrm{adv}} = 1 - \phi|_{\mathrm{adv}}\,, \\ \Delta W_s &= (1 - \phi|_{\mathrm{adv}})\,(W_s|_{\mathrm{adv}} - W_f|_{\mathrm{adv}})\,, \\ \Delta W_f &= \frac{\rho_s}{\rho_f}(1 - \phi|_{\mathrm{adv}})\,(W_s|_{\mathrm{adv}} - W_f|_{\mathrm{adv}})\,. \end{aligned} \tag{A34}$$

In the numerical implementation, the reaction updates are relaxed in time using the characteristic time scale of melting Δt_{M}, which defines how quickly the porosity and partial water contents change to reach equilibrium. In addition, because the melting and equilibration typically occur at a shorter time scale than melt and solid motions, we divide the time step (that is equal to the advection time step) into several (at least 10) sub-steps. The updates are then computed iteratively over these sub-steps using a forward Euler method with the initial value equal to the “advective” solution. The changes of the partial water contents, porosity and temperature due to the reaction terms are then added point-wise to the “advective" solutions. For more details on time stepping and on treatment of reaction terms, see the ASPECT Manual (Bangerth et al., 2024b).

https://doi.org/10.5194/egusphere-2026-4958
Preprint. Discussion started: 3 September 2026

Table A1. Notation and parameter values.

Symbol	Meaning	Values	Unit
A	activation energy factor for solid viscosity	150	$\mathrm{kJ\,mol^{-1}}$
α	porosity factor for solid viscosity	20	—
c_p	heat capacity at constant pressure	1250	$\mathrm{J\,kg^{-1}K^{-1}}$
D	characteristic spacing of pores	10^{-3}	m
$\dot{\boldsymbol{\epsilon}}$	solid strain rate tensor		$\mathrm{s^{-1}}$
η_f	shear viscosity of melt		Pa s
η_s	shear viscosity of solid		Pa s
η_0	solid viscosity prefactor	10^{12}	Pa s
η_b	bulk viscosity of solid		Pa s
$\mathbf{g}$	gravity acceleration	10	$\mathrm{m\,s^{-2}}$
Γ	melting rate (mass-based)		$\mathrm{kg\,m^{-3}s^{-1}}$
Γ_s	reaction rate for solid water content		$\mathrm{s^{-1}}$
Γ_f	reaction rate for melt water content		$\mathrm{s^{-1}}$
k_ϕ	permeability		$\mathrm{m^2}$
k_0	permeability prefactor	0.01	—
k_T	thermal conductivity	3	$\mathrm{W\,m^{-1}K^{-1}}$
ϕ	volumetric melt fraction (porosity)		—
ϕ_{mass}	mass melt fraction		—
p_c	compaction pressure		Pa
p_f	melt pressure		Pa
R	universal gas constant	8.31	$\mathrm{J\,mol^{-1}K^{-1}}$
ρ	density		$\mathrm{kg\,m^{-3}}$
ρ_s	density of solid	2800	$\mathrm{kg\,m^{-3}}$
ρ_f	density of melt	2400	$\mathrm{kg\,m^{-3}}$
ΔS	entropy change due to melting	300	$\mathrm{J\,kg^{-1}K^{-1}}$
t	time		s, yr
Δt_{M}	characteristic melting time scale	1000	yr
T	temperature		K, °C
$\mathbf{u}_s$	velocity of solid		$\mathrm{cm\,yr^{-1}}$
$\mathbf{u}_f$	velocity of melt		$\mathrm{cm\,yr^{-1}}$
W	bulk water content of partially molten material		wt% H_2O
W_s	partial water content of solid		wt% H_2O
W_f	partial water content of melt		wt% H_2O